COMITATO NAZIONALE PER L'ENERGIA NUCLEARE
Laboratori Nazionali di Frascati

LNF-75/63(R)
18 Dicembre 1975

A. Małecki, J. M. Namysłowski and A. Reale: HEAVY ION COLLISIONS AT INTERMEDIATE ENERGIES: ELASTIC SCATTERING, COULOMB EXCITATION AND NUCLEON TRANSFER REACTIONS. -

Servizio Documentazione
dei Laboratori Nazionali di Frascati del CNEN
Casella Postale 70 - Frascati (Roma)

Laboratori Nazionali di Frascati del CNEN
Servizio Documentazione

LNF-75/63(R)
18 Dicembre 1975

A. Małecki,[o] J. M. Namysłowski[x] and A. Reale :

HEAVY ION COLLISIONS AT INTERMEDIATE ENERGIES: ELASTIC SCATTERING, COULOMB EXCITATION AND NUCLEON TRANSFER REACTIONS. -

ABSTRACT. -

A review of standard and new methods used in describing heavy-ion processes is given in connection with a proposal of a heavy-ion machine at the National Laboratories of Frascati. The experimental proposal of the machine is shown and is compared with other machines. Introductory remarks are made about the semiclassical method, and more emphasis is put on the DWBA scheme, with some account of its approximations and shortcomings. An extensive presentation of the eikonal type methods for dealing with heavy ion processes is made in view of the applicability of these methods in the energy region 10-150 MeV/nucleon.

(o) - From Institute of Nuclear Physics, Cracow (Poland.

(x) - Institute of Theoretical Physics, Warsaw University, Warsaw (Poland).

CHAPTER 1 - THE OUTLOOK OF INTEREST IN HEAVY ION COLLISIONS. -

1.1. - Introductory remarks. -

There are several reasons why one wants to scatter heavy ions, inspite of their complicated structure. Before describing them let us, however, make some introductory remarks concerning the characteristic features of heavy-ion collisions.

The most important property is the smalness of the wavelength λ in the relative motion of two heavy ions; λ is small in comparison with the characteristic distance D. The ratio λ/D is of the order 10^{-2}. Small λ makes it reasonable to talk about the Newton trajectories. Ions moving on these trajectories are repelled from each other by strong Coulomb field, and for not too high energies we can introduce the notion of a distance of closest approach in a head-on collision for the backward scattering. We denote this distance by 2a, and illustrate it in Fig. 1.1.

FIG. 1.1. - Projectile Z_p approaching the target Z_t with the relative velocity v moving in a head-on collision.

From the Newton law we get:

$$a = \frac{Z_p Z_t e^2}{\mu v^2} , \tag{1.1}$$

where μ is the reduced mass of two ions.

Taking the ratio of a to $\lambda = \hbar(\mu v)^{-1}$, we get:

$$\frac{a}{\lambda} = \eta = \frac{Z_p Z_t e^2}{\hbar v} . \tag{1.2}$$

This ratio η is an important, large, dimensionless parameter, and it enters the well-known formula for the Rutherford scattering cross section in the following way:

$$\left(\frac{d\sigma}{d\Omega}\right)_R = \frac{1}{4}\eta^2(\mu v)^{-2}\sin^{-4}\frac{\theta}{2} . \tag{1.3}$$

Varying the laboratory energy of projectile ion one gets to the so-called Coulomb barrier, which is the maximum safe bombarding energy before we enter the field of nuclear force. Denoting the Coulomb barrier by E_{CB}, we get an expression for it by equating the centre of mass relative motion energy with the electrostatic energy at the distance of closest approach:

$$E_{CB}\left(1+\frac{A_1}{A_2}\right)^{-1} = Z_1 Z_2 e^2 (R_1 + R_2 + \Delta)^{-1} , \tag{1.4}$$

where A, Z, R are ion's mass number, charge and radius, respectively, and $\Delta \approx 3$ fm. Taking $R = 1.41\ A^{1/3}$, $Z \approx 0.49\ A(1+A^{2/3}(166)^{-1})^{-1}$, we get in Fig. 1.2 the plot of the Coulomb barrier E_{CB}, in MeV for different charges of projectile, as a function of the charge of target.

For energies below the Coulomb barrier ions are strongly repelled by the Coulomb force, while for energies above the Coulomb barrier there is a strong absorption at very small distances which also prevents us to see such final ions which deeply penetrated one into the other. Therefore, the heavy ion collision is a peripheral, or surface process, and a typical distance D which characterizes the smallest interesting distance above the Coulomb barrier is roughly the sum of two radii of the ions. For an arbitrary energy the definition of D is:

$$D = \begin{cases} 2a & , \text{ for } E < E_{CB} \\ R_1 + R_2 & , \text{ for } E > E_{CB} \end{cases} . \qquad (1.5)$$

As an example we show in Fig. 1.3 the large dimensioneless parameter $D \cdot \lambda^{-1}$ for scattering of argon on mercury as a function of the projectile energy.

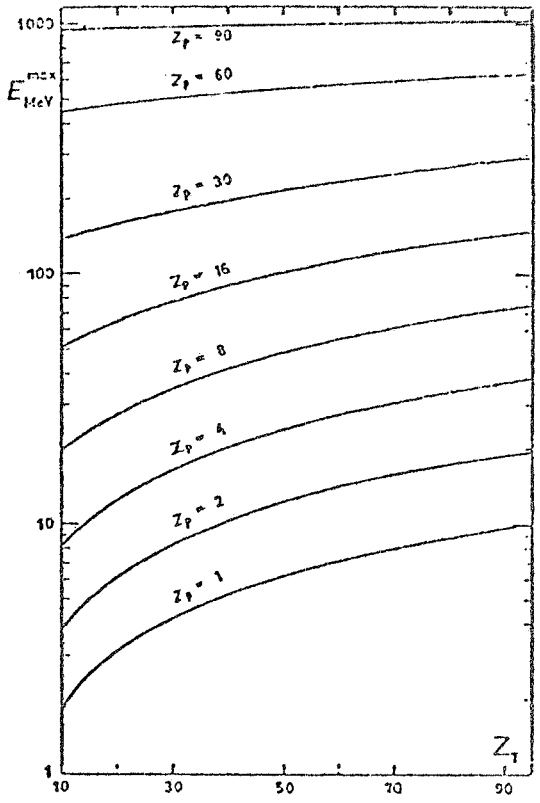

FIG. 1.2. - Maximal bombarding energy E_{CB} is shown as a function of the target charge Z_t for different projectile charges Z_p. From ref. (1.1).

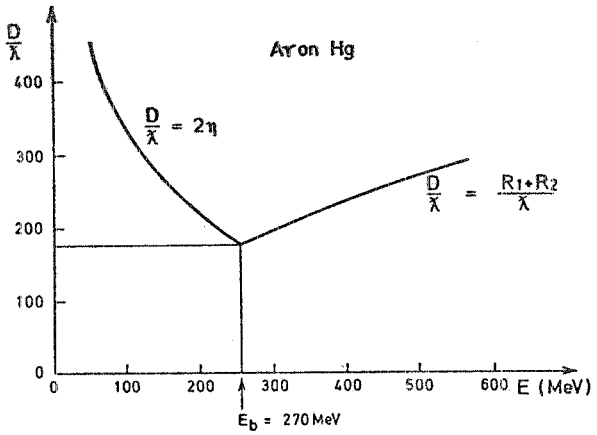

FIG. 1.3. - The ratio between the characteristic length D and the wavelength in the relative motion for argon projectiles on mercury as a function of bombarding energy in MeV. For energies below the Coulomb barrier ($E_{CB} \approx 270$ MeV), D is taken to be the distance of closest approach in a head on collision, while for $E > E_{CB}$, D is taken to be the sum of the nuclear radii. From ref. (1.2).

The fact that $D \cdot \lambda^{-1}$ is very large (≥ 200) implies that the semiclassical, WKB or eikonal descriptions have a very good chance to work well. These simple methods, which yield the analytic or almost analytic form of expressions for the cross-sections, constitute the basic framework for the study of dynamics in the heavy-ion collisions.

1.2. - Outlook of interest in heavy-ion collisions. -

The present day experiments with heavy-ion beams are done either below the Coulomb barrier or just above it, around 10 MeV/nucleon, or at much higher energies from about 200

MeV/nucleon up to 2000 MeV/nucleon. The intermediate energy region in the gap from 10 MeV/nucleon to 150 MeV/nucleon could be available at the Frascati Laboratories. Different phenomena will be manifested in this energy range and for illustration we reproduce in Fig. 1.4 a drawing made by W. J. Swiatecki[1.3]. We note that in the gap region nuclear physics

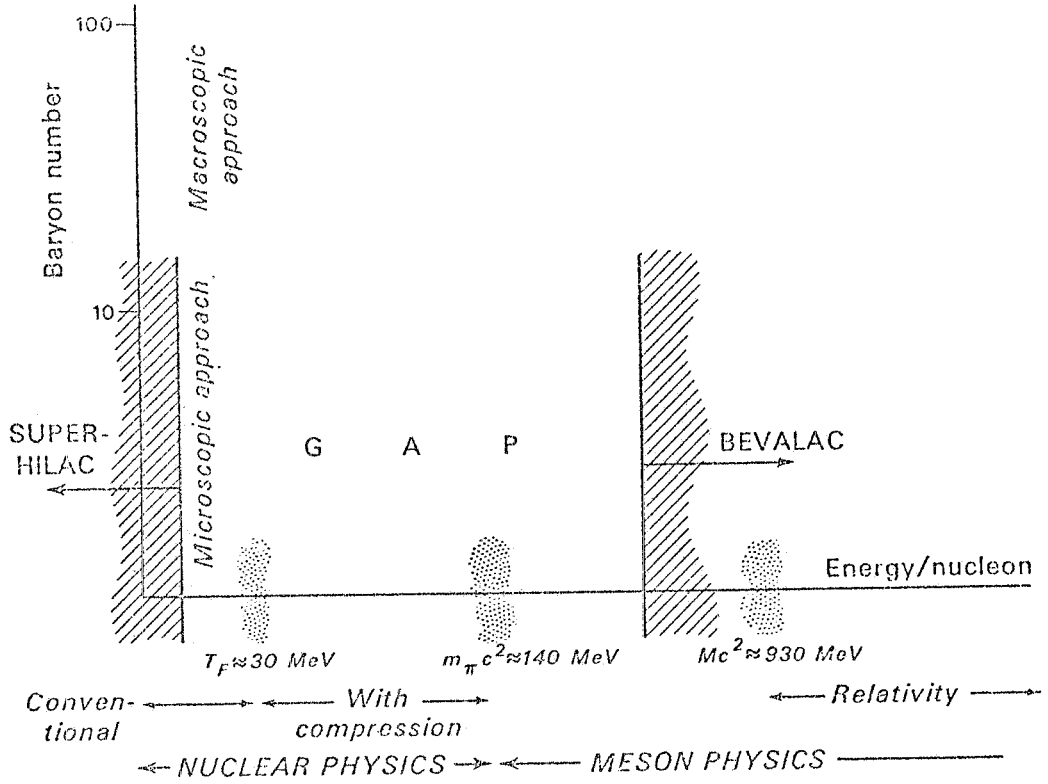

FIG. 1.4 - From ref. (1.3).

will be studied under some special compressed conditions, and that it will get overlapped with the meson physics. Studying heavy-ion physics in this range of energy one would also aim at a common view on heavy ion processes in the law, intermediate and high energies. This requires to focus our attention both on the conventional heavy-ion processes met in the low energies, and on the new phenomena.

We may distinguish three energy regions where the reasons of scientific interest are somewhat different:

A) Phenomena below the Coulomb barrier[1.4].

Here the interaction is essentially of the electromagnetic type and it is known. We are expecting in this energy region phenomena of Coulomb excitation and, in particular, for very heavy nuclei, Coulomb excitation of states with high spins or the possibility of fission of the interacting nuclei (Coulomb fission).

B) Phenomena above the Coulomb barrier.

In this energy region we can study the mechanism of the elastic scattering or transfer reactions between nuclei, the inelastic excitation of residual nuclei or the formation of compound nucleus. Let us examine briefly these points:

B.1. - Elastic scattering[1.5] and transfer reactions[1.6].

This topic shall be elaborated in detail in Chapters 3, 4 and 5, after presentation of the experimental facilities in Chap. 2. Chap. 3 serves as an introduction to the subject and in

Chapters 4 and 5 we emphasize the eikonal methods for dealing with the elastic scattering and transfer reactions, since we feel that they can provide a uniform way of interpreting the data at different energies, particularly at the intermediate and high energies.

B. 2. - Nuclear spectroscopy.

Most commonly, the nuclear structure studies with heavy-ion beams are done at low, sub-Coulomb energies. There, the Coulomb wave functions are excellent approximations, and spectroscopic factors can be obtained with good precision. Increasing the energy of projectile we allow for a more complicated interplay of the nuclear and Coulomb force, and necessarily the formalism becomes more involved. However, also the cross section for the transfer reactions increases. Kinematical selection rules favour large angular momentum transfer, and large cross section enable us to reach nuclear states with high spin which are difficult to populate otherwise. In fact, at energies around 10 MeV/nucleon there was noted high selectivity to high spin states[1.7].

B. 3. - Departure off stability line.

Another area of the nuclear structure study with heavy ions is the search for properties of nuclides far off the stability line. The large excess of neutrons, which can be found in the products of heavy-ion collisions, enable us to get extra conditions for the nuclear structure models of the stable nuclei.

B. 4. - γ spectroscopy and the behaviour of high spin states.

We note that the products of heavy-ion collisions can acquire very large angular momenta up to 100 units of h. These objects after evaporating a few neutrons, send out cascades of γ rays, which can be used to learn about the properties of very high spin states. The nuclear systems "rotating" with very large spin are put under extreme conditions. The nuclear structure studies have to be extended to this entirely new regime, since the change of nuclear structure may be very drastic[1.8].

C) Phenomena much above the Coulomb barrier.

In this energy region it is possible to predict many phenomena as complete fusion between the interacting nuclei or the exchange of many nucleons and/or of great amount of energy (deep inelastic processes). If exchange of nucleons will take place new nuclear species will be created: the outcoming nuclei can carry out in a more or less stable way a great number of neutrons or protons so that on can hope to study new nuclei far from the stability valley. This method has been already used at Dubna where many new isotopes have been observed (e. g. $_{16}O^{24}$), by bombarding heavy ion targets with light projectiles (O, Ne, A, etc.) at 10-15 MeV/nucleon and observing that the outcoming projectile was enriched in neutrons.

Of course it would be interesting to extend such measurements to much higher energies. On the other hand, a high excitation energy of the final fragmenta can determine quite interesting thermodynamical conditions of nuclear matter whose behaviour will depend on "macroscopic" properties as viscosity, compressibility, etc. Let us consider briefly the various phenomena:

C. 1. - Complete fusion.

In connection with this topic there are many open questions: can the high angular momentum of the fusion nucleus preclude its existence? The high rotation energy, in fact, can produce a great deformation of the nucleus which will increase its tendency to fissioning. This tendency depends also on the momentum of inertia of the nucleus which is different for a fluid or rigid body. In this respect it is important to better explore the so-called "Yrast" line. When a nucleus is an "Yrast" state all the excitation energy E is in the form of rotation energy; below the line $E = E(J)$ we cannot find excited states of spin J. The shape of this curve depends on the properties of the excited nucleus and its knowledge is of great interest.

C. 2. - Deep inelastic processes.

When two nuclei do not reach some characteristic distance then the complete fusion cannot be obtained. If a projectile is not completely absorbed, it can loose kinetic energy, or it can loose or gain electric charge and mass. The projectile which is slown down in such a way will leave the collision region not as consequence of the initial momentum but because of the Coulomb repulsion. These "deep inelastic processes" are sometimes called strongly damped collisions because of the strong damping of the energy degrees of freedom. In the exit channel a large amount of energy is converted into the excitation energy. Huizenga[1.9] gives the following characteristics of the strongly damped collisions: 1° - the exit fragments have generally masses not far from the masses of projectile and target, although if the target mass is large enough the excited heavy fragment will sequentially fission; 2° - the kinetic energies of fragments correspond to Coulomb energies for charge centers of highly deformed fragments, analogous to that for fission fragments; 3° - the angular distributions are strongly peaked, as in the direct processes. The cross-section for these processes may be a major part of the total cross-section at intermediate energies.

C. 3. - Nuclear fragmentation.

The fragmentation of a nucleus in nuclear collisions seems to be an interesting problem not only at relativistic energies, but also around 100-200 MeV per nucleon. Some results indicate[1.10] that the fragmentation cross-section is independent of energy in a large range from 0.1 to 2.0 GeV/nucleon, which is surprising and deserves further studies. In spite of its limited intensity the Frascati machine could contribute quite immediately to the analysis of such processes through the study of the energy and angular distributions of the fragments.

C. 4. - Unusual processes.

During the interpretation of a high energetic nucleus with a heavy target violent compression waves (shock waves) may be generated[1.11]. The high temperature reached in the shock zone allows the creation of nucleon isobars and the pionization. The meson production renders the hadronic matter less "stiff" so that great compression can be attained. The dense, hot and highly isobaric matter which occurs in the shock waves may have quite different properties than the normal nuclear matter[1.12].

The unusual situation appears also for quantum electrodynamics if the sum of the projectile and target charges exceeds 137[1.13].

An electron, carried by heavy ion, behaves quite differently in an overcritical Coulomb field than it does in the ordinary bound state. During the time of collision of too heavy ions a superheavy molecule emerges. In such molecule, electron feels attraction coming from both ions which are very close, and in its unbound state it must coexist with the sea of positrons. Vacuum gets polarized and the emission of positrons can be viewed as the decay of vacuum in overcritical fields. One can study the X-ray spectroscopy for superheavy molecules and learn new aspects of quantum electrodynamics in very strong fields. We meet here an example of spontaneously broken symmetry, and get link with the currently discussed unified theories of weak and electromagnetic interactions. It is notable that the study of heavy ion collision may shed some light on such fundamental questions, as the interaction of elementary particles, and even models of elementary particles, which are recently viewed also as complicated objects, namely as bags of quarks.

REFERENCES. -

(1.1) - K. Alder, in Oak Ridge Heavy Ion Summer Study, Oak Ridge, Tennessee, 1972 (ed. by S. T. Thornton).
(1.2) - R. A. Broglia and A. Winther, Phys. Reports 4C, 153 (1972).
(1.3) - W. J. Swiatecki, in 2nd High Energy Heavy Ion Summer Study, July 1974, Report LBL-3675 (1974), p. 349.
(1.4) - K. Alder and A. Winther, Coulomb excitation. A collection of reprints with an introductory review (Academic Press, 1966).
(1.5) - T. W. Donnelly, J. Dubach and J. D. Walecka, Nuclear Phys. A232, 355 (1974); A. Dar and Z. Kirzon, Nuclear Phys. A237, 319 (1975).
(1.6) - Symposium on Heavy Ion Transfer Reactions, Argonne 1973, Report PHY-1973B (1973).
(1.7) - N. Anyas-Weiss et al., Phys. Reports 12C, 203 (1974).
(1.8) - Z. Szymanski, in Proceedings of the Intern. Conf. on Nuclear Physics (eds. J. de Boer and H. J. Mang), Munich (1973), p. 402.
(1.9) - N. Huizenga, in Proceedings of the 7th Masurian School in Nuclear Physics, Nukleonika 20, 291 (1975); Phys. Rev. C11, 1265 (1975).
(1.10) - K. Kristiansson et al., in Proceedings of the 14th Intern. Cosmic Ray Conf., Munich, (1975), vol. 7, p. 2358.
(1.11) - H. G. Baumgardt et al., Z. Phys. A273, 359 (1975).
(1.12) - T. D. Lee and G. C. Wick, Phys. Rev. D9, 2291 (1974).
(1.13) - W. Greiner et al., Phys. Rev. Letters 28, 1235 (1972).

CHAPTER 2 - HEAVY ION ACCELERATING MACHINES AND EXPERIMENTAL FACILITIES. -

2.1. - Heavy ions machines. -

In these years the various scientific communities have considered with a great interest the convenience of building heavy ion accelerating machines. The main purpose is to get heavy ion beams of great intensity and high energy.

It is well known that the usual electrostatic accelerators have already provided a great deal of informations on the structure of nuclei but they are strongly limited to energies either below or just above the Coulombian barrier. On the other hand high energy accelerators like the Bevalac are limited to very high relativistic energies, say (300-2500) MeV/nucl so that intermediate energies are actually not covered by the existing machines. This is a great disadvantage for our knowledge of nuclear matter, because many interesting phenomena are expected in that region[2.1]. This limitation will be overcome by the future machines so that the way is open to new discoveries in the field of nuclear physics.

Of course the "ideal" heavy ion accelerating machine should be able to give ion beams of all nuclear species from H to U, of great intensities, say $> 10^{11}$ particles/second in a wide energy range from ~ 1 MeV/nucl to $\sim 10^4$ MeV/nucl with a very good energy resolution and possibly long duty-cycles to perform coincidence experiments. As matter of fact, in order to avoid increasing too much the financial efforts and the technical difficulties each laboratory is forced to plan the construction of a specific machine, which will allow to do physics in some specific energy range or with some restriction on the kind of projectiles.

What kind of machine is then more convenient depends on the physical interest; e.g. low energy very intense beams are needed to look to excitation levels of nuclei, while one has to use relativistic energy beams to study, say, the nuclear fragmentation phenomena.

The general way of obtaining ion beams is sketched in Fig. 2.1 for circular accelerators.

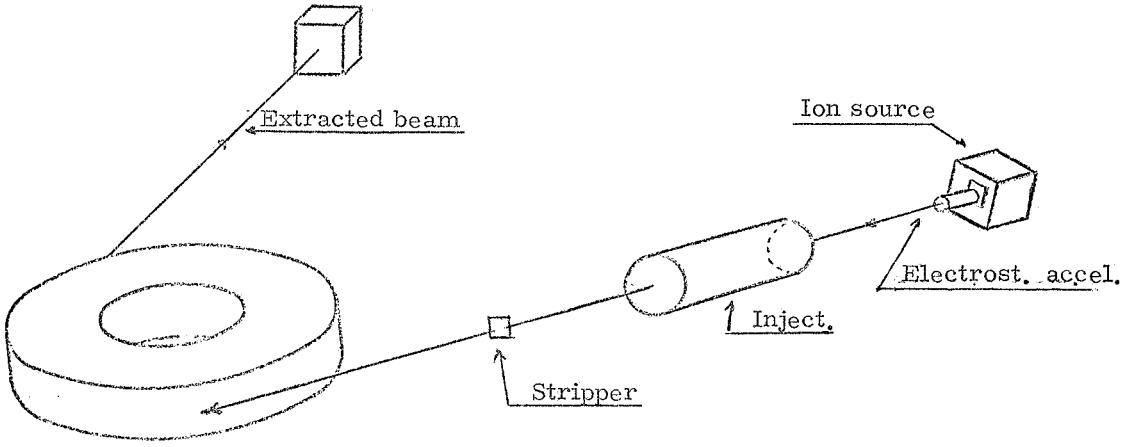

FIG. 2.1 - Schematic layout of an heavy ion circular accelerator.

As it is shown, charged atoms coming from the source are injected in some kind of pre-accelerator which can be of an electrostatic type (Van der Graaff, Tandem) or a linac or a small cyclotron or both. Depending on the type of injector, the ion sources have to produce either negative ion beams,(Heinicke sources, duoplasmatron, etc.) i.e. atoms to which an electron has been "added" (as for a tandem) or positively charged ions (Pennig sources), i.e. atoms which have been spoiled (stripped) of one or more orbital electrons (as for cyclotrons or linac injectors).

Usually ions, after having been accelerated to some energy by the injector, are again

stripped in T (by making their traverse a very thin foil of material), so that their final effective charge is $\bar{Z} \simeq Z$. After the second stripping they are injected in to the circular ring and accelerated, by a suitable system of accelerating cavities or in some other way, to achieve the final energy. In the usual cyclotrons or synchrotrons the final energy per nucleon is given by:

$$\varepsilon_f = \frac{E_f}{A} = K B^2 R^2 \left(\frac{\bar{Z}}{A}\right)^2 ,$$

where K is some numerical factor, B and R are the magnetic field and the magnetic radius of the machine, respectively.

One can see from the previous formula the convenience of obtaining ionized atoms of great $\bar{Z}$ in order to arrive to high final energies. Unfortunately, there are some limitations of the charge state $\bar{Z}$ that one can get from the sources or in the stripping process; the difficulties are greater for heavier atoms. Of course it would be the best to have fully ionized atoms, but this is not so easy because the ionization efficiency in the stripping process in T is limited depending on the ion energy at the output of the injector and on the considered nucleus.

The average charge state $\bar{Z}$ depends, in fact, on the nucleus energy according to the formula[2.2]:

$$Z = c\sqrt{Z \cdot \varepsilon_{inj}} , \qquad 0.1 < \frac{\bar{Z}}{A} < 0.4 ,$$

where c is a numerical constant depending if the stripper is a solid or a gaseous target, and Z and ε_{inj} are the atomic number and energy/nucl at the output of the injector, respectively. One can see that high energy injectors would be convenient to reach high ionization states $\bar{Z}$, but they are of course too much expensive. Just to give an idea of the expected charge state $\bar{Z}$, we report in Table 2.1 the ionization states that one can get by stripping in T, assuming as injector a 16 MV tandem as it was considered in ref. (2.3), for the Frascati synchrotron.

TABLE 2.1

I	A	ε_{inj}	Z	$\bar{Z}$
H	1	32	1	1
C	12	9.3	6	6
N	14	9.15	7	7
O	16	7	8	8
F	19	5.9	9	9
S	32	4.5	16	14
Cl	35	4.1	17	15
Ni	58	2.76	28	22
Zn	64	2.5	30	22
Br	79	2.22	35	25
I	127	1.88	52	32

One can see that is not so difficult to have light nuclei fully stripped ($\bar{Z} = Z$), but for heavier nuclei $\bar{Z}$ is usually less than Z.

For what is concerning the intensities of the output beams, these are of course, depending on the features of the ion sources, the injector and final accelerator acceptances, the possibility of producing a good vacuum (better than 10^{-8} mm Hg) inside the circular rings, which is relevant to a good transmission during the acceleration cycle, stripper efficiency and so on. A great technical progress is expected in the next years in the heavy ion performances

both of negative and positive ion sources.

For sake of clearness it is convenient to divide the new accelerators projects in to three classes:

a) New electrostatic accelerators, which can give very intense ion beams, of low energy/nucleon say $E/A \leq 10$ MeV/nucl, but of very great energy resolution. The intensity of the outcoming beams from these machines are greater than 10^{12} particles/sec and the energy resolution is of the order of 10^{-4}. The usual Van de Graaff or Tandem generators are working in this way.

b) Cyclotrons or Linac accelerators are meant to be useful for getting very intense beams ($\geq 10^{11}$ particles/sec) within an energy range between, say, 10-100 MeV/nucl.

c) Circular machines, like synchrotrons, which can give high energy beams, say 100-3000 MeV/nucl with typical intensities $\leq 10^{10}$ particles/sec.

The construction of all the devices is achieved either by constructing "ex novo" the machines or by conversion of machines already existing. As we said the main difficulty of all then projects is to balance the financial difficulties with the goal of high energy - high intensity ion beams.

Among the various existing projects, one could mention, as examples of the type b) projects the French national project GANIL, the UNILAC of Darmstadt, the Japanes NUMITRON, and in Italy the project of a superconducting cyclotron(2.4).

One has to consider as projects of type c) the Bevalac of the Berkeley Laboratories, the AGS of Brookhaven, the French Saturne II, and probably the Serpukov protosynchrotron(2.5).

Few years ago in Frascati the proposal has been made of converting the 1.1 GeV electronsynchrotron into an ion accelerator(2.6). Two possibilities were originally considered: either to use linac or Tandem as injector. While the second one cannot be considered (no Tandem is available for the moment), the first version is still possible even in an enlarged version with respect to the old one. In Fig. 2.2 we report a graph of the energies of some projects including the Frascati one, while in Tables 2.2 and 2.3 we tried to summarize the world situation concerning all the projects.

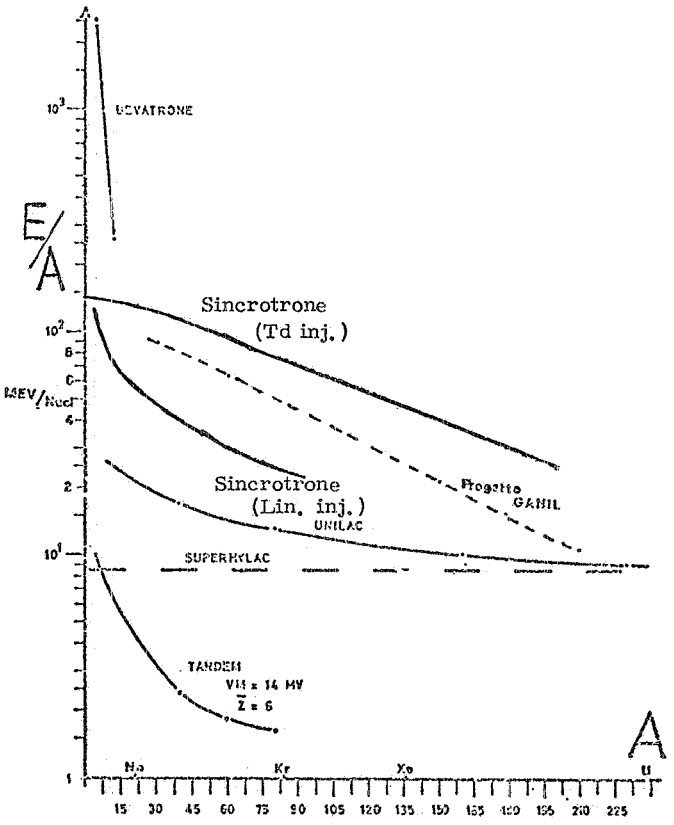

FIG. 2.2 - Energy/nucl vs atomic mass for different heavy ion machines.

TABLE 2.2

Type of machine	Site	MeV/nucleon	Nuclei	Status
Linac supercond.	Argonne, Karlsr.	— 10	→ U	proposed
Hylac	Los Alamos		→ U	proposed
Superhylac	Berkeley		→ U	OK
Unilac	Darmstadt	30-8	→ U	1975
Bevalac	Berkeley	2500-250	→ A	1974
Saturne II	Saclay	200-2000	→ Ne	proposed
Ganil	Saclay	≤100	→ U	construct.
Alice (Cycl.)	Orsay	5	→ Kr	OK
Cyclotron	Dubna	7	→ Xe	OK
Cyclotron	Oak Ridge	10		proposed
Cyclotron	Italy			
Tandem	USA	(6-10) MV		
Tandem	France			
Tandem	Netherland			
Tandem	Germany			
Tandem	England	50 MV		construct.
Tandem	Rumania	7.5 MV		OK
Tandem	Italy	16 MV		1976
Pelletron	Israel	14 MV		OK
Pelletron	Australia	14 MV		OK
Pelletron	Brasil	22 MeV(p)		OK

TABLE 2.3

	Tandem	Linac	Cyclotron and Synchrotron
E/A	≤ 10 MeV/nucl	~ 10 MeV/nucl	~ (100-1000) MeV/nucl
Z	any	~ any	~ any
Inten.	μA or fraction of μA	(10-100) μA Es: 1 μA of U	$10^9 - 10^{12}$ p/sec
duty cyc.	1	(25-100) %	(10-20) %
Δp/p	$< 10^{-4}$	(0.3-1) %	(0.1-0.5) %

It is worthwhile to write as in Table 2.4 the gross features of the beams coming out from the few ones of the considered circular accelerators, in order to give the relevant informations for planing of future experiments.

As one can see from Table 2.4 one can expect that in the next years then will be available very intense ion beams of all possible energies between few MeV/nucl up to GeV/nucl, with an energy resolution of (0.1-0.2)% and very good optical properties.

TABLE 2.4

Project	Energy/nucleon (approx.)		Intensity part/sec	Beam energy
Frascati Synchrotron	130 → 20	He → Au	5×10^{9}-5×10^{7}	~ 0.2 %
Superconducting magnet	50 → 15	He → Ur	$\sim10^{11}$	~ 0.1 %
GANIL	100 → 10	He → Ur	$\sim10^{12}$	0.1 %
UNILAC	20 → 7	He → Ur	$\geq10^{12}$	0.25 %
Saturne II	200 - 200	He - Ne	10^{9}-10^{10}	0.3 %

2.2. - Experimental facilities.-

To perform an experimental program concerning the phenomena we discussed in section 1.2, we have to provide a suitable experimental apparatus for measuring angular and energy distributions of the emitted particles and their mass numbers, at different projectile energies.

Let us consider first two body elastic or inelastic reactions at energies of the projectile nuclei around 100 MeV/nucl like in the Frascati or Milano projects

$$A + B \rightarrow C + D. \qquad (2.1)$$

Rates for reactions (2.1) depend on many factors as beam intensity, target thickness, angular acceptance of the experimental apparatus and, of course, the cross section of the considered processes at these energies. One cannot increase too much the useful target thickness, in order to limit energy losses and Coulombian scattering of the emitted particles in the target. Generally an accetable value for the target thickness is in the range between (0.2--2) mg/cm^2. In these conditions at least for lighter ions the momentum resolution will be comparable with the momentum resolution of the incoming beam reported in Table 2.4.

It is in fact necessary to have experimental apparatus of good angular and energy resolution to allow the measurement of many of the reactions we have listed in section 1.2. For two body reaction an experimental apparatus like the Saclay energy loss spectrometer[2.7], that has an energy resolution of $\sim$ 100 keV, would be fully adequate to most of the reactions we mentioned, apart from its high cost. Of course one has also to consider less expensive experimental solution like the so called Palevsky spectrometer[2.8] in some modified version as the one of ref. (2.3) that is reported in Fig. 2.3. As one can see from Fig. 2.3 the magnet C is necessary to bend the primary beam, while the two H magnets are used to analyse the emitted particles. The trajectories of the particles in the spectrometer are measured by a system of multiwire proportional chambers or drift chambers. The emission angle of the emitted particles can be varied by a displacement of the target along the beam direction of motion and keeping fixed the position of the spectrometer.

With such a system one can show[2.3] that energy and angular resolution can be obtained of the order of

$$\delta E/E \simeq \pm 0.3\,\%, \qquad \delta\theta \simeq \pm 2 \text{ mrad},$$

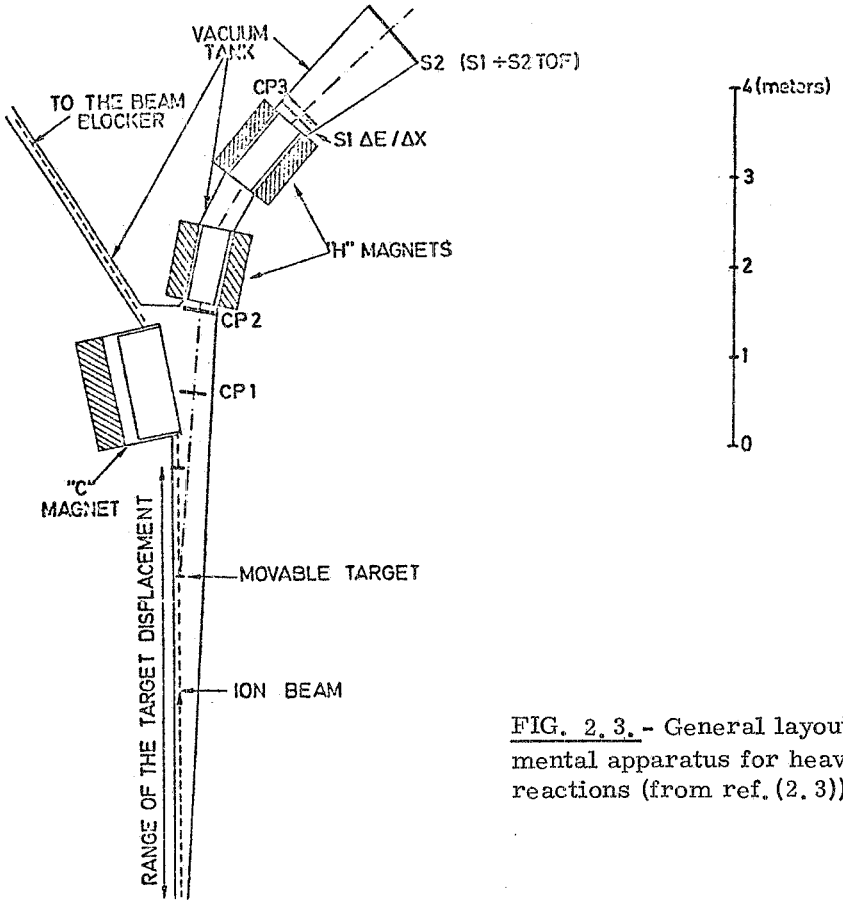

FIG. 2.3. - General layout of an experimental apparatus for heavy ion two-bodies reactions (from ref. (2.3)).

in an (laboratory system) angular interval between say 4^{o} and 20^{o}, with a spectrometer acceptance of the order of $(1\text{-}2)\times10^{-3}$ sterad and a momentum acceptance of ~ 20 MeV/c.

Typical values of the involved momenta:

$$p \simeq 7 \text{ GeV/c} \qquad \text{for} \quad O^{16} \text{ nucleus with } E/A = 100 \text{ MeV/nucl.}$$

As an example of the expected distribution we quote from ref. (4.2) a typical elastic scattering spectrum of O^{16} or C^{12} at $E_{lab} = 168$ MeV that is at about 10 MeV/nucl in the laboratory system (see Fig. 4.8 - pag. 41).

For studying many body reactions like

$$A + B \rightarrow C + D + E + \ldots$$

in this energy range one can think about experimental devices which are typical of high energy particle experiments. There are mainly MWPC and scintillators arrangements, in a closed or open configuration around the target, to get the emission angles and energies of the emitted particles, their specific energy loss dE/dx, and times of flight. Of course for same type of reactions it is also necessary to try to reconstruct also the masses of the emitted particles. For light ions a complete mass separation is possible[2.4], for heavier ions it is more difficult and single reactions should be examinated separately.

REFERENCES. -

(2.1) - 2nd High Energy Heavy Ion Summer Study, Lawrence Berkeley Laboratory (July, 1974).
(2.2) - Ch. Schmelzer, in Linear Accelerators (ed. by Lapostolle and Septier), p. 1036.
(2.3) - Rapporto del gruppo di studio sulla conversione dell'elettrosincrotrone di Frascati in acceleratore di ioni, (LNF, Servizio Documentazione, 1975).
(2.4) - GANIL, Rapport du group de travail pour l'Accelerateur National a Ion lourds (1973); E. Acerbi, C. Birattari, M. Castiglioni, L. Grillo, C. Pagani, M. Puglisi, F. Resmini e G. Tagliaferri, Proposta per lo studio di un progetto di ciclotrone per ioni pesanti con magnete a bobine superconduttrici, Rapporto INFN, Sezione di Milano (1975).
(2.5) - Proposal 32: High intensity uranium beams from the superhilac and the Bevalac, Lawrence Berkeley Laboratory; Proposal of conversion of the Brookhaven AFS in to an ion accelerator, Report Interet des Ions lourds relativistes à Saturne II, Saturne II Entreprise comune CEA 1N2P3, report int. (1975).
(2.6) - G. Brautti, Convertibilità dell'elettrosincrotrone di Frascati per l'accelerazione di ioni, Rapporto dell'Istituto di Fisica dell'Università di Bari e Sottosezione INFN di Bari (1972); G. Brautti, T. Letardi, G. Maggipinto e A. Reale, Il sincrotrone di Frascati come acceleratore di ioni: modifiche strutturali e programmi. Possibili sviluppi del progetto, Presentato al Convegno del 16-17 Maggio 1974 in Frascati, Rapporto LNF-74/49 (1974).
(2.7) - J. Thirion, Proc. Intern. Conf. on Nuclear Physics, München 1973 (Eds. J. de Boer and H. J. Mang) (North Holland/American Elsevier), pag. 781.
(2.8) - J. L. Friedes, R. Sutter, H. Palevsky, G. Bennet, G. Igo, W. D. Simpson, R. L. Stearms and D. M. Corley, Nuclear Instr. and Meth. 54, 1 (1967); R. J. Sutter, G. Bennet, J. Fisher, J. L. Friedes, H. Palevsky, R. Persson, G. Igo and W. D. Simpson, Nuclear Instr. and Meth. 54, 71 (1967).

CHAPTER 3 - STANDARD METHODS OF DESCRIBING HEAVY ION PROCESSES. -

Two methods are commonly used for describing the heavy ion elastic scattering and transfer reactions. One is based on the semiclassical concepts, and the other one is a quantal method. We shall illustrate the semiclassical method on the example of elastic scattering, and the quantal method on the examples of one-and two-nucleon transfer reactions. In such cases the standard quantal method is known as the "Distorted Waves Born Approximation" (DWBA) formalism.

3.1. - The semi-classical method. -

Let us consider elastic scattering, say, of the ^{16}O ions on ^{58}Ni. We take as given the central potential V(r), describing the interaction of the two nuclei. For the Newtonian motion on an orbit in the field V(r) we evaluate a quantity named the deflection function. It is:

$$\theta(b) = \pi - 2 \int_{r_o}^{\infty} dr \, \frac{b}{r^2} \left[1 - \frac{b^2}{r^2} - \frac{V(r)}{E} \right]^{-1/2} , \qquad (3.1)$$

where r_o is the turning point, i.e. the classical distance of closest approach, b is the impact parameter, related to the angular momentum l by $kb = l$, $E = k^2(2\mu)^{-1}$ and μ is the reduced mass. θ is the angle by which a classical particle with energy E and angular momentum l (thus also with a fixed impact parameter b) gets deflected in the central potential V(r).

To get more acquainted with the deflection function let us consider for the moment V(r) as given by the pure Coulomb interaction. In Fig. 3.1 we plot the deflection function, and note a unique correspondence between b and $\theta(b)$. A different character has the deflection function for V(r) being the Woods-Saxon potential. It is plotted in Fig. 3.2 and we note that

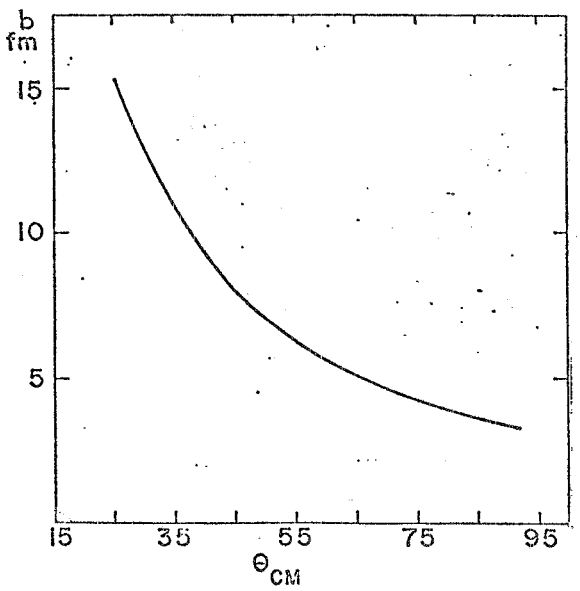

FIG. 3.1. - Deflection function $\theta(b)$ arising from a Coulomb potential - from ref. (3.1).

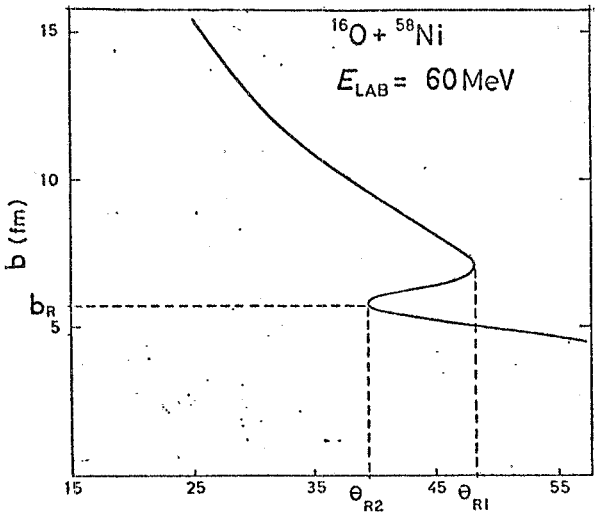

FIG. 3.2 - Deflection function $\theta(b)$ for the scattering of ^{16}O on ^{58}Ni at 60 MeV - from ref. (3.1). The real potential was taken in the Woods-Saxon form:

$V(r) = V_R \left[1 + \exp\left(\frac{r-R}{a}\right) \right]^{-1}$ with $V_R = -7$ MeV, $R = 9.65$ fm, $a = 0.6$ fm.

for some angles there are three values of impact parameter. All of them must be included. In Fig. 3.2 appear also another two points around which the deflection function has the parabolic shape. Scattering angles corresponding to these points are called rainbow scattering.

In the pure classical theory the differential cross section can be obtained from the derivative of the inverse function of $\theta(b)$. We have:

$$\left(\frac{d\sigma}{d\Omega}\right)_{classical} = \frac{b\, db}{\sin\theta\, d\theta} \quad . \tag{3.2}$$

The semiclassical method uses some concepts of the classical theory, but also incorporates some quantal features. To get the prescription for the evaluation of $d\sigma/d\Omega$ in the semiclassical model we begin from the standard quantal formula for $d\sigma/d\Omega$. We write:

$$\begin{aligned} d\sigma/d\Omega &= \left|f(\theta)\right|^2 \\ f(\theta) &= \frac{i}{2k} \sum_{l=0}^{\infty} (2l+1)(1 - e^{2i\delta_l})\, P_l(\cos\theta) \, . \end{aligned} \tag{3.3}$$

In order to evaluate the phase-shifts δ_l's we take advantage of the fact that for heavy ion scattering the relatively large reduced masses give rise to large values of $k = \sqrt{2\mu E}$ even at moderate energies E. The large value of the wave number k justifies the use of an approximate treatment of the Schrödinger equation known as the WKB (Wentzel-Kramers-Brillouin) method.

The WKB approximation is discussed in many-textbooks, see e.g. ref. (3.3). We will only state the final result and discuss its physical background. The basic assumption is that, at large k the main effect of the potential is to modulate the phase of the wave function, hence the radial solutions of the wave equation may be tried in the form:

$$\mu_l(r) = \exp\left(\pm i\, \phi(r)\, k\right) .$$

If we assume further that the distance d over which the potential V(r) changes significantly is large compared with the wave-length $\lambda = k^{-1}$, i.e. $kd \gg 1$, one may neglect $d^2\phi/dr^2$. The third assumption in the WKB method is the condition that the radial wave function vanishes at the so-called turning point r_o, determined through the relation:

$$\frac{k^2}{2\mu} = V(r_o) + \frac{(l+\frac{1}{2})^2}{2\mu r_o^2} \quad . \tag{3.4}$$

This boundary condition clearly has a motivation borrowed from classical mechanics where a particle cannot penetrate past the point in which the kinetic energy equals the effective potential (real potential plus centrifugal energy) barrier.

The WKB method gives the following expression for the l-th partial scattering phase shift:

$$\delta_l^{WKB}(k) = \frac{1}{2}\pi(l+\tfrac{1}{2}) - kr_o + \int_{r_o}^{\infty} \left[k(r) - k\right] dr \quad , \tag{3.5}$$

where:

$$k(r) = k\left[1 - (l+\tfrac{1}{2})^2 (kr)^{-2} - V(r)\, E^{-1}\right]^{1/2} \quad ,$$

and the turning point r_o is determined from $k(r_o) = 0$.

The WKB formalism may be extended to complex potentials such as the optical-model potential(3.3). In this case r_o becomes complex and the integral in (3.5) is in the complex plane from the complex turning point to real infinity.

A difficulty arises if there exist multiple solutions for r_o. A possible choice is to take then the solution with the largest real part and the smallest negative imaginary part corresponding to reflection at the first barrier. The ambiguity can be a source of error only for a very few partial waves which are tunneling through the first potential barrier. At energies near the Coulomb barrier this occurs only for the lower partial waves where the error is reduced by the absorptive part of the optical potential. For energies above the Coulomb barrier these ambiguities are less important and disappear completely at high energies.

Comparing Eqs. (3.5) and (3.1) it is appropriate to notice the very close relationship between a derivative of the WKB phase shift and the classical deflection function. We have:

$$2\frac{d\delta_l^{WKB}}{dl} = \vartheta(l) , \qquad (3.6)$$

with the relation $kb = l+1/2$ kept in mind.

An example of the partial phase-shifts is given in Fig. 3.3 for elastic scattering $^{18}O + ^{120}Sn$ at 100 MeV(3.4). One can see that only partial waves with 50 l 70 are contributing to the scattering amplitude. The relatively small interval of large values of l is a typical feature for scattering of heavy ions.

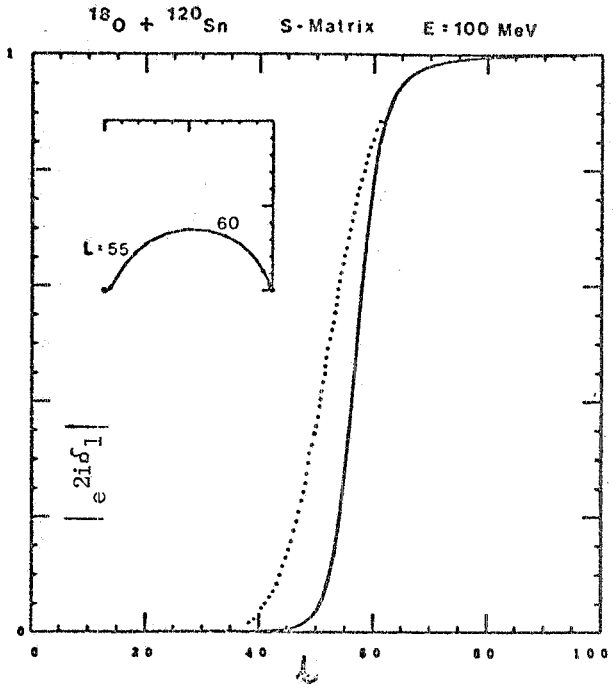

FIG. 3.3. - The amplitude of $e^{2i\delta_l}$ for elastic scattering $^{18}O + ^{120}Sn$ at 100 MeV (Ref. (3.4)), corresponding to the Woods-Saxon potential $V(r) = (V_R+iV_I)\left[1+\exp(\frac{r-R}{a})\right]^{-1}$, with parameters $V_R = -40$ MeV, $V_I = -15$ MeV, $a = 0.45$ fm, $R = 1.31$ fm $(A_1^{1/3}+A_2^{1/3})$. Dashed line corresponds to $V_R = 0$ and shows by comparison how the real potential sucks high l's into the absorbing region.

The smallness of the interval of the effective l's is the result of strong absorption at the surface and of attractive force which sucks high angular momentum orbits into the absorbing region. The large values of l arise because of large radii of heavy ions and large values of k; roughly the half value of $|e^{2i\delta l}|$ occurs at $l_o = kR$, R being the radius of the potential.

The WKB method helps us in getting information about the phase-shift, but to evaluate the cross-section we must know the amplitude $f(\theta)$, i.e. we must perform the summation in Eq. (3.3). This may be simplified as follows. Because of strong absorption the sum over

partial waves is determined mainly by the terms with large l. Hence we can replace $P_l(\cos\theta)$ by the asymptotic expression for large l:

$$P_l(\cos\theta) \approx \left[\frac{\pi}{2}(l+\frac{1}{2})\sin\theta\right]^{-1/2} \sin\left[(l+\frac{1}{2})\theta + \frac{\pi}{4}\right] , \tag{3.7}$$

omitting from considerations $\theta = 0, \pi$.

Substituting this in (3.3) and replacing the sum by an integral (thus assuming that the phase-shift is a smooth function of l) one obtains:

$$f(\theta) \approx -(2\pi k \sin\theta)^{-1/2} \int_0^\infty dl\,(l+\frac{1}{2})^{1/2}(e^{i\varphi_+} - e^{i\varphi_-}) , \tag{3.8}$$

where:

$$\varphi_\pm = 2\delta_l \pm (l+\frac{1}{2})\theta \pm \frac{\pi}{4} .$$

Finally we evaluate the integral in Eq. (3.8) using the method of stationary phase. We get that the main contribution comes from such values of l, denoted by l_i, for which the phases $\varphi_\pm$ have extrema. This is so because near extremum the exponents vary slovly, hence in this region the exponential factors will not cancel. Thus we have the condition:

$$\left(\frac{d\varphi_\pm}{dl}\right)_{l=l_i} = 0 , \tag{3.9}$$

from which follows (see Eqs. (3.6) and (3.8)) the relation:

$$\pm\theta = \theta(l_i) , \tag{3.10}$$

$\theta(l_i)$ being the classical deflection function.

Having stationary points we expand δ_l around them up to the second order, and explicitly evaluate the integral over l. From each stationary value we get a contribution to the scattering amplitude

$$f(\theta) = \sum_i f_i(\theta) ,$$

with

$$f_i(\theta) = -k^{-1}(l_i+\frac{1}{2})^{1/2}\left[2\sin\theta\left|\frac{d^2\delta_l}{dl^2}\right|_{l=l_i}\right]^{-1/2} \exp i\,\alpha(l_i) ,$$

$$\alpha(l_i) = \left[2\delta_l - 2(l+\frac{1}{2})\frac{d\delta_l}{dl} - \frac{\pi}{4}\left(2 - \frac{d^2\delta_l}{dl^2}\Big/\left|\frac{d^2\delta_l}{dl^2}\right| - \frac{d\delta_l}{dl}\Big/\left|\frac{d}{dl}\right|\right)\right]_{l=l_i} . \tag{3.11}$$

The differential cross section is obtained in the semiclassical method as:

$$\left(\frac{d\sigma}{d\Omega}\right)_{\text{semi-classical}} = \left|\sum f_i(\theta)\right|^2 . \tag{3.12}$$

Therefore the interference effects which are absent in the classical expression are induced in the semi-classical formula.

In Fig. 3.4 there is a plot of the ratio

$$\left(\frac{d\sigma}{d\Omega}\right)_{semicl} / \left(\frac{d\sigma}{d\Omega}\right)_{R}$$

as the continuous line, and it is compared with a plot of the same ratio evaluated exactly (broken line). Here "exact" means that we solve numerically the Schrödinger equation and found out the phase shifts δ_l. The agreement is very good.

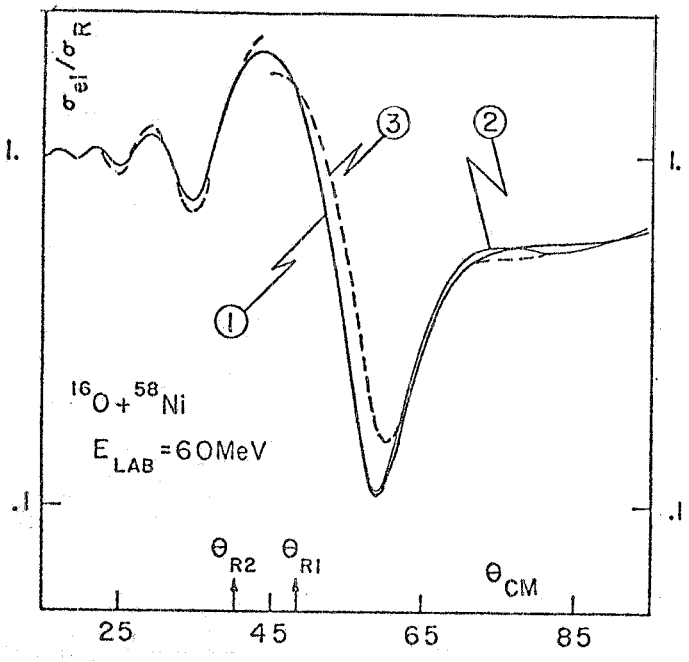

FIG. 3.4 - Elastic cross-section for scattering of ^{16}O on ^{58}Ni at 60 MeV. The real potential parameters are given in caption of Fig. 3.2. Curve 1 represents the exact calculations; curve 2 the semi-classical one; curve 3 the result obtained by stationary phase method.

The semi-classical method can be extended over to inelastic scattering with excited final states of the target and to one-or-more-nucleon transfer reactions. The agreement with the experimental data is quite good, however, in cases when the final state differs from the initial one, more assumptions are needed to write down an expression for the cross section. In such situation the classical trajectory corresponding to the relative motion of ions in the initial state is deferent from the trajectory in the final state, and some averaging procedure is needed. One must also deal with an imaginary part of the optical potential, and evaluate reaction matrix elements from a coupled set of 1-st order differential equations, following from the time dependent Schrödinger equation. This set of equations is solved numerically with the appropriate initial conditions. The whole procedure is rather involved, but the agreement with the experimental data is very good. We end here our presentation of the semiclassical method and refer to Broglia et al.[3.5], for more details.

3.2. - The quantal method. -

The second standard method of treating heavy ion processes is the quantal method. For elastic scattering it is known as the optical potential method and for inelastic scattering and transfer reactions as the distorted waves Born approximation (DWBA).

3.2.1. - Optical model.

In the elastic case one parametrizes real and imaginary parts of potential, most often assumed in the form of Woods-Saxon potential, adds the Coulomb potential, solves numerically the Schrödinger equation, and looks for the best parameters fitting differential cross section.

As an example we consider scattering of the ^{16}O ions on ^{60}Ni at 60 MeV laboratory energy. The experimental data[3.7] are well fitted by the following total potential:

$$V(r) = V_N(r) + V_C(r) \ , \tag{3.13}$$

with the nuclear part of the potential, V_N, a Woods-Saxon optical-model potential

$$V_N(r) = \frac{V_R}{1+\exp((r-R_{0R})/a_{0R})} + \frac{iW_I}{1+\exp((r-R_{0I})/a_{0I})} \ , \tag{3.14}$$

and with a Coulomb potential V_C of the form

$$\begin{aligned} V_C(r) &= (Z_1 Z_2 e^2/2R_C)(3-r^2/R_C^2) \qquad r < R_C \ , \\ &= Z_1 Z_2 e^2/r \qquad\qquad\qquad\quad r > R_C \ , \end{aligned} \tag{3.15}$$

which is extension to the case of heavy ion scattering of the potential due to a point charge on a uniformly charged sphere. Presumably a more correct for two heavy ions would be the potential of two uniformly charged spheres. However, because of nearly total absorption near the origin, where the difference in the various Coulomb potentials is largest, the scattering cross-sections are fairly insensitive to the choice of the model Coulomb potential.

The values of the parameters used for the fit were:

$$\begin{aligned} V_R &= -25 \text{ MeV} \ , \\ W_I &= -15 \text{ MeV} \ , \\ R_C &= R_{0I} = R_{0R} = 1.3(A_1^{1/3} + A_2^{1/3}) \text{ fm} = 8.365 \text{ fm} \ , \\ a_{0R} &= a_{0I} = 0.5 \text{ fm} \ . \end{aligned}$$

Fig. 3.5 shows the fit; moreover it gives a comparison of the "exact" calculation of the differential cross-section (made with ABACUS II) and the WKB method[3.6]. All results

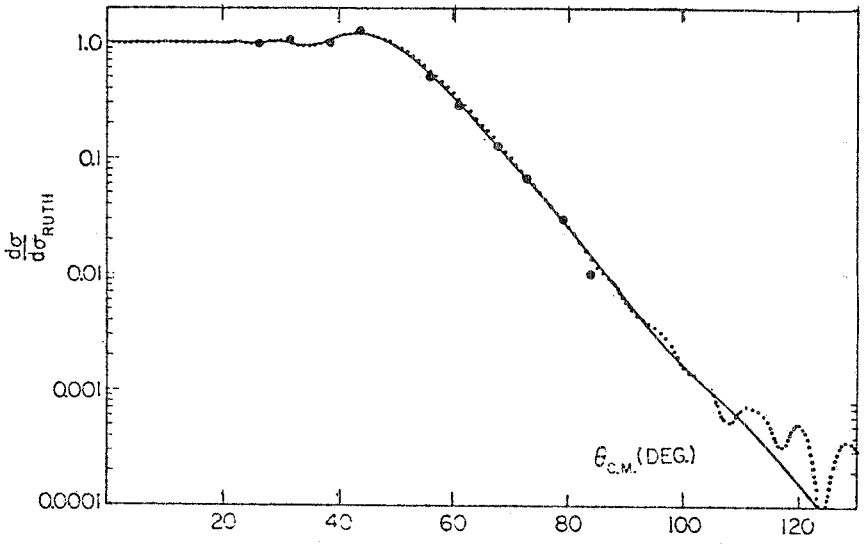

FIG. 3.5. - The reaction $^{60}Ni(^{16}O, ^{16}O)^{60}Ni$ at lab energy of 60 MeV - from ref. (3.6). Experimental points (large dots) taken from ref. (3.7), and calculations using ABACUS II (solid line) and WKB (dotted line).

are displayed in ratio to the Rutherford cross-section. As can be seen the agreement is quite good over the entire curve.

In general the WKB approximation agrees well with the optical model cross-section for energies and angles of major interest, i.e. $E_{cm} > 40$ MeV and angles over which $d\sigma/d\Omega_{Ruth}$ changes by three decades[3.6]. The WKB method fails for energies which are excessively low or angles which are excessively large. Thus in the example shown in Fig. 3.5 beyond 100^{o} the WKB curve shows diffraction peaks with maxima in $d\sigma/d\Omega_{Ruth} \approx 5 \times 10^{-4}$ and with a much larger maximum at 180^{o} ($d\sigma/d\Omega_{Ruth} \approx 5 \times 10^{-3}$). On the contrary the exact calculation continues to decrease, levelling off at $d\sigma/d\Omega_{Ruth} \approx 8.2 \times 10^{-6}$ at 180^{o}.

At high energies the WKB method, being fairly insensitive to values of k, may, however, be numerically superior than the exact procedure the effectiveness of which rapidly decreases for large k. For large k the numerical integration of the Schrödinger equation becomes, because of the fine integration meshes required, a very difficult task.

3.2.2. - The DWBA method.

Let us now pass to transfer reactions and show some details of the evaluation of differential cross section within the DWBA method[3.8]. We denote by t the transferred subsystem and by c_1, c_2 the cores with which t is making up a bound state in the initial and final state, respectively. These bound systems we denote as $a_1 = (c_1, t)$ and $a_2 = (c_2, t)$ and our transfer reaction is:

$$(c_1, t) + c_2 \longrightarrow c_1 + (c_2, t) \ , \qquad (3.16)$$

or

$$a_1 + c_2 \longrightarrow c_1 + a_2 \ .$$

The basic three bodies c_1, c_2 and t are depicted in Fig. 3.6 at vertices of a triangle,

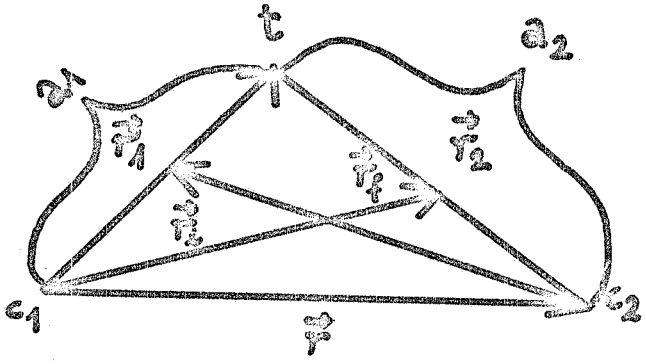

FIG. 3.6 - The vector diagram for the transfer reaction $(c_1, t) + c_2 \rightarrow c_1 + (c_2, t)$.

their relative distances are the sides of triangle, and $\vec{r}_i$, $\vec{r}_f$ denote the relative distance between the projectile and target in the initial and final state, respectively.

In the DWBA method one assumes:

a) The interaction between projectile and target, before or after the transfer took place, can be described in the initial and final state in terms of optical potential $U_{a_1c_2}$ and $U_{c_1a_2}$ respectively;

b) These optical potentials do not differ too much from the interaction between cores $V_{c_1c_2}$;

c) The matrix element for a transfer process is proportional to the residual interaction, which is sandwiched between the states which are products of bound system wave functions of a_1 and a_2, and distorted waves in the initial and final states, respectively.

Then the differential cross section for transfer process can be schematically written as:

$$\frac{d\sigma}{d\Omega} \approx S_1 S_2 \left| \langle \chi_f^{(-)}(\vec{k}_f, \vec{r}_f)\, \phi_2 \right| V_r \left| \chi_i^{(+)}(\vec{k}_i, \vec{r}_i)\, \phi_1 \rangle \right|^2 , \qquad (3.17)$$

where S_1, S_2 are the so called spectroscopic factors, uniquely defined by the initial and final bound state structures. They measure the strength of a given state of t in the bound systems a_1, a_2 respectively; χ_i, χ_f are distorted waves describing the relative motion of a_1 and c_2 or a_2 and c_1 interacting via $U_{a_1 c_2}$ or $U_{a_2 c_1}$ respectively; ϕ_1, ϕ_2 are the bound state wave functions of t in a_1, a_2 respectively; V_r is the residual interaction, describing interaction which is not included in distorted waves. It depends on a representation, and in the post-representation it is:

$$V_r = V_{c_1, a_2} - U_{c_1\, a_2} = (V_{c_1\, t} + V_{c_1\, c_2}) - U_{c_1\, a_2} \approx V_{c_1\, t} . \qquad (3.18)$$

Here, V_{AB} denotes an effective interaction between A and B and we have used $V_{c_1\, c_2} \approx U_{c_1\, a_2}$.

The matrix element in Eq. (3.17) contains 6-dimensional integral, very unpleasant to deal on a computer. To simply calculation especially below the Coulomb barrier one usually makes some further approximations within the DWBA scheme:

a) Localization in the strong Coulomb field. Such field favours large core-core distances, and therefore ϕ_2 can be reasonably approximated by its asymptotic form

$$\phi_2 \approx N_2\, h_{l_2}^{(1)}(i\sqrt{2m B_2}\, r_2)\, Y_{l_2 \lambda_2}(r_2) , \qquad (3.19)$$

where N_2 is the normalization constant, B_2 is the binding energy of t in a_2, m the reduced mass in the (t, c_2) system, $h_l^{(1)}$ being the Hankel function.

b) no-recoil, based on the smallness of the mass of transferred particle with respect to the mass of the bound system of this particle with the core. Looking at Fig. 3.6 we write:

$$\chi_i^{(+)}(k_i, r_i) = \chi_i^{(+)}(\vec{k}_i, \vec{r} - \frac{m_t}{m_{a_1}} \vec{r}_i) \approx \chi_i^{(+)}(\vec{k}_i, \vec{r}) ,$$

$$\chi_f^{(-)}(k_f, r_f) = \chi_f^{(-)}(\vec{k}_f, (1 - \frac{m_t}{m_{a_2}})\vec{r} - \frac{m_t}{m_{a_2}} \vec{r}_1) \approx \chi_f^{(-)}(k_f, (1 - \frac{m_t}{m_{a_2}})\vec{r}) \qquad (3.20)$$

$$\approx \chi_f^{(-)}((1 - \frac{m_t}{m_{a_2}})\vec{k}_f, \vec{r}) .$$

The last step is true if the function χ_f depends only on the product of momentum and the position variable, as it is in the case of pure Coulomb wave functions. The no-recoil approximation enables us to replace a 6-dimensional integral by a product of two 3-dimensional integrals.

Next, one of the 3-dimensional integrals is replaced by a one-dimensional integral and a sum over angular momentum, using a property of the Hankel function which was put in instead of ϕ_2. The final formula for the one-nucleon transfer differential cross-section (3.9) is:

$$\frac{d\sigma}{d\Omega} = 4\pi \frac{m_i m_f}{(2\pi h^2)^2} \frac{k_f}{k_i} \frac{2a_2+1}{(2c_2+1)(2j_2+1)} S_{j_1 l_1} S_{j_2 l_2} \left| A_{l_1} \right|^2 \left| N_2 \right|^2 .$$

$$\cdot \sum_{l\lambda} \left\langle j_1 \tfrac{1}{2} l 0 \middle| j_2 \tfrac{1}{2} \right\rangle \left| T_{l\lambda}(\theta) \right|^2 \quad , \tag{3.21}$$

where :

m_i, m_f are reduced initial and final masses ;

j_1, j_2 are total angular momenta of nucleon bound in a_1, a_2, respectively; similarly l_1, l_2 ;

$$A_{l_1} = \int dr_1 r_1^2 j_{l_1}(i\sqrt{2m B_2 \hbar^{-2}}\, r_1)\, V_{nc_1}(r_1)\, \mu_{l_1}(r_1) \ ;$$

$$T_{l\lambda}(\theta) = \int d^3r\, \chi_f^{(-)*}((1 - \frac{m}{m_{a_2}})\vec{k}_f, \vec{r})\, h_{l_2}^{(1)}(i\sqrt{2m B_2 \hbar^{-2}} r)\, Y_{l\lambda}(r)\, \chi_i^{(+)}(\vec{k}_i, \vec{r}) \ ;$$

$\mu_{l_1}(r)$ is the radial wave function of nucleon in the (n, c_1) bound state.

The values of l are bounded by the following conditions :

$$|l_1 - l_2| \leq l \leq l_1 + l_2 \ ,$$
$$|j_1 - j_2| \leq l \leq j_1 + j_2 \ ,$$
$$(-1)^{l_1 + l_2} = (-1)^l \ .$$

This formalism was developed by Buttle and Goldfarb[3.9] and was very successful in interpreting many experiments. For illustration we show in Fig. 3.7 results obtained for the total cross section, with spectroscopic factors in agreement with the shell-model predictions.

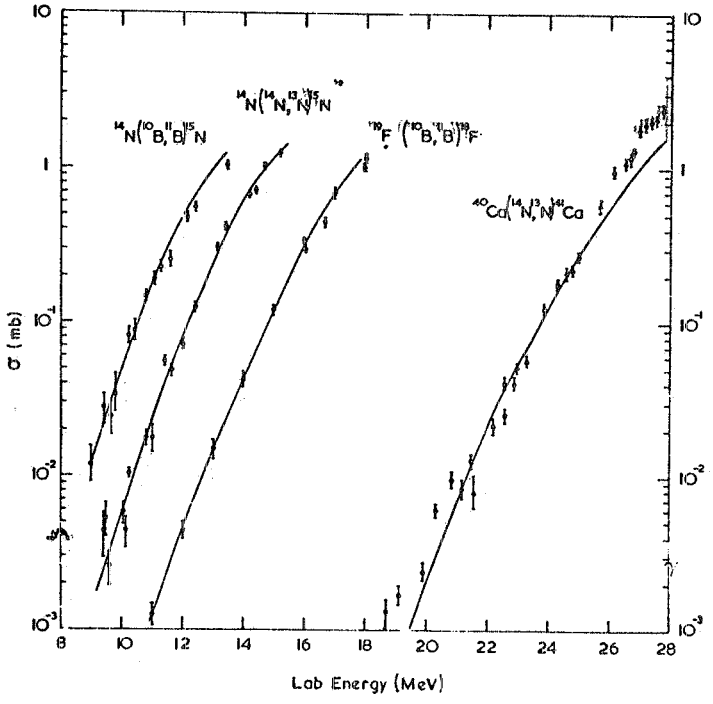

FIG. 3.7. - The total cross-section of the one-nucleon transfer reactions (from ref. (3.8)).

Another example of a very good fit of the DWBA, no-recoil, finite-range method is given in Fig. 3.8. for one-nucleon transfer processes at different laboratory energies.

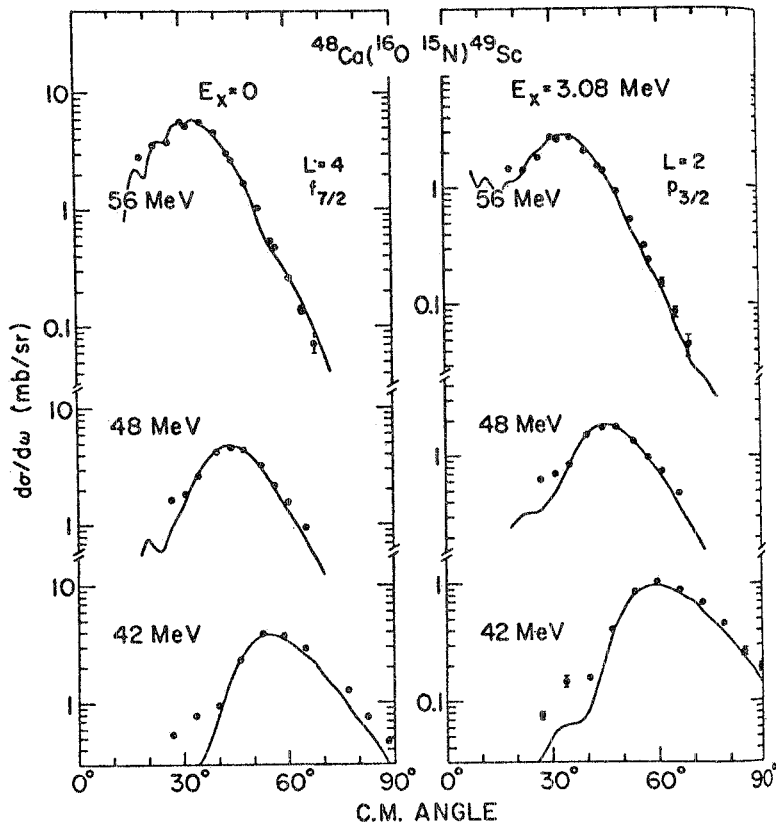

FIG. 3.8. - Angular distributions for the $^{48}Ca(^{16}O, ^{15}N)$ reaction to the $1f_{7/2}$ ground state and $2p_{3/2}$ excited state in ^{49}Sc. The solid lines represent DWBA calculations performed with the no-recoil code (from ref. (3.10)).

There are three characteristic features to note :

i) the angular distributions have a bell shape ;
ii) the bell becomes narrower for higher energies ;
iii) the maximum of the bell is moving forward for higher energies.

The bell-shape angular distributions are connected with the phenomenon of grazing collision. It arises because of the strong, repelling Coulomb force on one side, and the strong nuclear absorption on the other side. The most favourable scattering angle for nucleon transfer is called the grazing angle, and in terms of classical trajectories it corresponds to well matched initial and final trajectories.

It should be pointed out that in order to get a good agreement of the DWBA fits with the experimental data it is often necessary to include extra normalization factors ranging up to 3.5.

3.3. - Difficulties of the standard methods. -

In spite of good fits obtained by the semiclassical and DWBA methods there are number of problems connected with these methods. We shall make only a few remarks about the semiclassical method, and concentrate our attention on the difficulties of the DWBA scheme.

For transfer reactions the semiclassical method finds difficulty in coping with different initial and final trajectories and some ad hoc averaging procedure is invoked to cure this disease. Troubles also arise in defining the phase in the semiclassical method. The WKB and stationary phase methods come with some help in defining the semiclassical phase, but with different initial and final trajectories it is only a heuristic argument, and in fact for the transfer reaction a definite phase must be assumed and can not be derived. There are also some recipies how to evaluate the cross section for the transfer processes, and geometrical mean value seems to be accepted, though, including the arbitrariness in phase, they do not follow from any physical assumptions. On computational side the difficulties are in coping with very many partial waves and solving of very many coupled sets of differential equations. It becomes a enormous task to carry out such calculations even on big computers, thus limitations or further approximations must be contemplated.

Troubles of the DWBA method are quite numerous. To start with let us remind that the DWTA amplitude is a first term of a divergent series, as shown by Greider and Dodd[3.11], within the 3-body formulation of rearrangement processes. For some processes like knock-out reactions it is possible to reformulate the infinite series in such a way that its term will be the t-matrix instead of the residual interaction V_r, and in this case one speaks about the DWBA amplitude. Such an amplitude is a first term of an infinite series which is generated by a kernel free of disconnected diagrams, thus it has a chance to be a convergent series, though the estimate of the importance of the 2-nd order and higher order terms contributions is a separate, unanswered question.

In practice within the DWBA method one makes several additional approximations and above the Coulomb barrier, where both the nuclear and Coulomb forces interfere one allows oneself for some change of parameters so that a good fit to the experimental data is achieved. Large ambiguities arise from not univocally defined parameters of the optical potential. Elastic scattering of ions in both initial and final states is needed as a separate set of data, but it does not fix up univocally the optical potential parameters. Even if these parameters are determined from a partial wave analysis of the elastic scattering they are changed in the DWBA numerical programs to get better fits to the transfer processes. For sub-Coulomb energies there is much less uncertainty than above the Coulomb barrier, because of the dominance of the known Coulombic wave functions.

Another source of discrepancies within the DWBA scheme is in the spectroscopic factors. They should be given by the nuclear structure theories, and may be looked at as predictions of the DWBA method, if a good fit to the cross section is found. In practice, there are sometimes found such predictions of the DWBA scheme, that the spectroscopic factors for different states do not agree with the nuclear structure predictions, even by factor 2 and then one cures the situation by speaking about the ratic of spectroscopic factors. The inconsistency in spectroscopic factors can be noted also if one compares the same factors found in different reactions. These discrepancies have tendency to increase with the increasing energy. Only for sub-Coulombic processes there is a small discrepancy in determining spectroscopic factors by the DWBA scheme.

An important problem of the DWBA method is the question of recoil, especialy for energies high enough above the Coulomb barrier. Bellow the Coulomb barrier the effect of recoil is small, and may be safely neglected. However, let us look at one-nucleon transfer reaction $^{11}B(^{14}N, ^{15}O)^{10}Be$ and watch the variation of the angular distribution with increasing energy. In Fig. 3.9 the solid line gives the prediction of no-recoil DWBA amplitude, while the broken line goes through the experimental points to guide the eye. For the laboratory energy 113 MeV the DWBA no-recoil amplitude gives quite a wrong prediction.

De Vries[3.13] among others, analyzed the influence of recoil and in Fig. 3.10 we show his study of recoil in the reaction $^{12}C(^{14}N, ^{13}C)^{13}N$ at 78 MeV laboratory energy. The featurless shape of experimental angular distribution, contrary to the oscillatory character of the no-recoil DWBA amplitude, can be understood if two contributions, arising in the case of included recoil, are added together. The oscillatory dips are filled up by maxima of the other contribution. It is nice for the DWBA method that the inclusion of recoil puts it back into agree

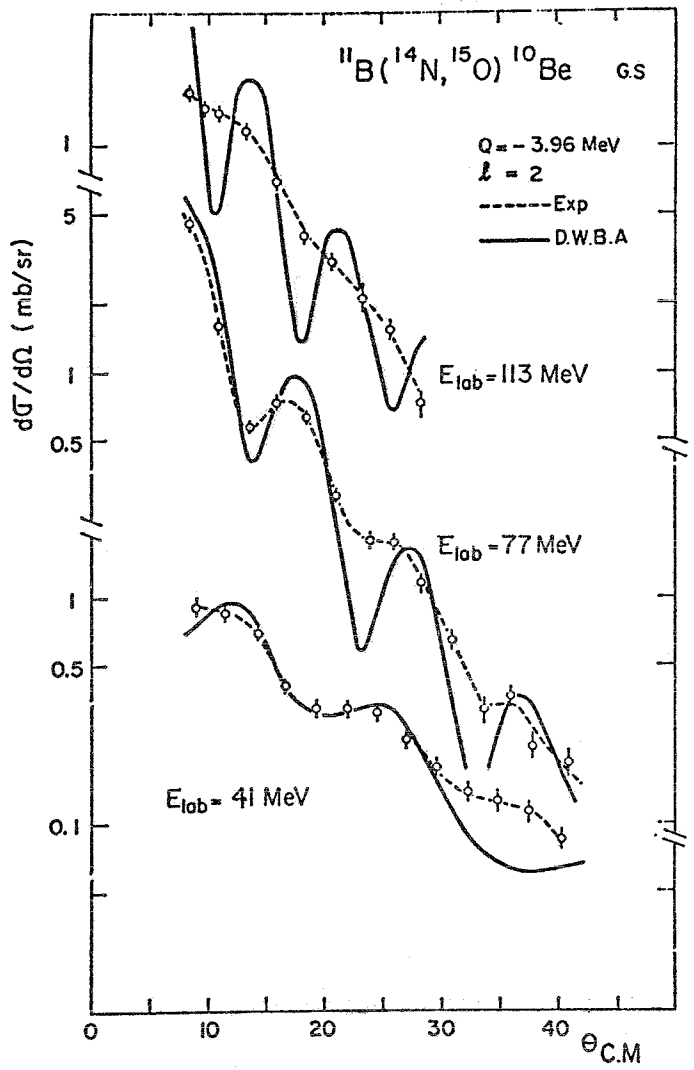

FIG. 3.9. - Differential cross sections for the reaction $^{11}B(^{14}N, ^{15}O)^{10}Be$ at 41, 77 and 113 MeV compared with "no-recoil" DWBA calculations, which predict increasing diffraction structure at the highest energy, in contrast to the featureless experimental data - from ref. (3.12).

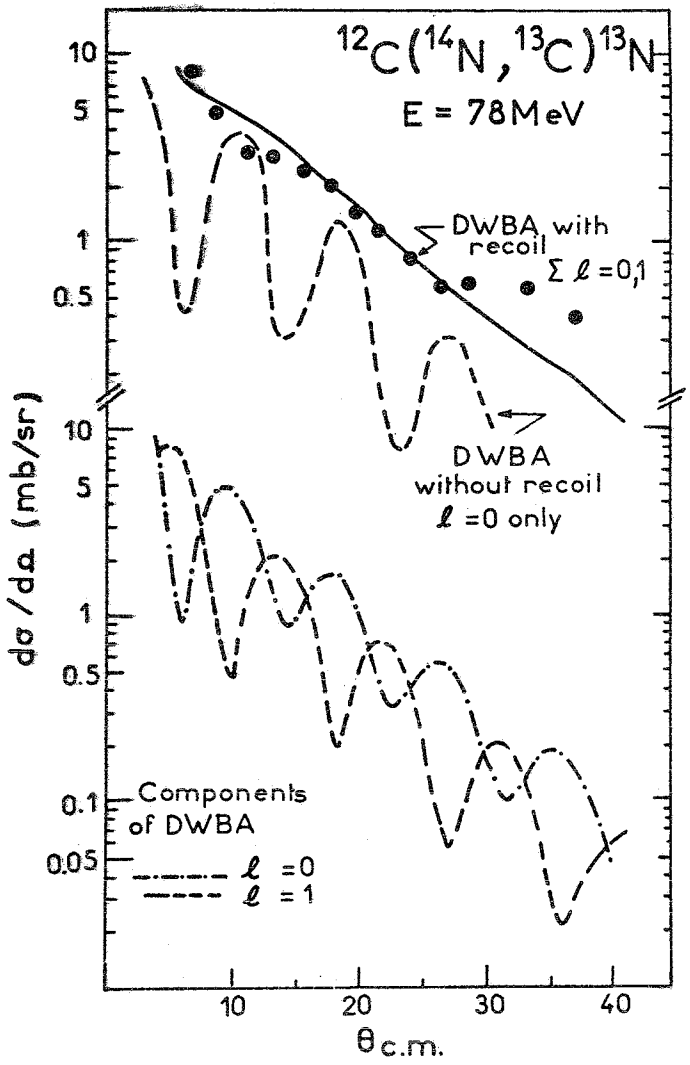

FIG. 3.10. - Theory (ref. (3.13)) and experiment (ref. (3.14)) for the $^{12}C(^{14}N, ^{13}C)^{13}N$ reaction.

ment with the data, but it forces us to use rather involved numerical programs, which can cope with 6-dimensional integrals.

The emphasis of recoil effects has also been made by Dodd and Greider[3.15] in their analysis of recoil damping in heavy ion transfer reactions. They found within the DWBA method that keeping the effect of finite mass of transferred particle resulted in the appearence of a recoil phase factor which gives strong damping of the diffraction oscillations. Due to this damping a featurless angular distribution appears which drops down as an inverse power of momentum transfer. Such behaviour is indeed suggested by the experimental data shown in Fig. 3.11, lying very well on the line q^{-4}. As stated by Dodd and Greider, in view of the simplification of their model and limitations of DWBA their result should not be taken as the whole explanation, but it suggests that at energies well above the Coulomb barrier recoil effects must be included.

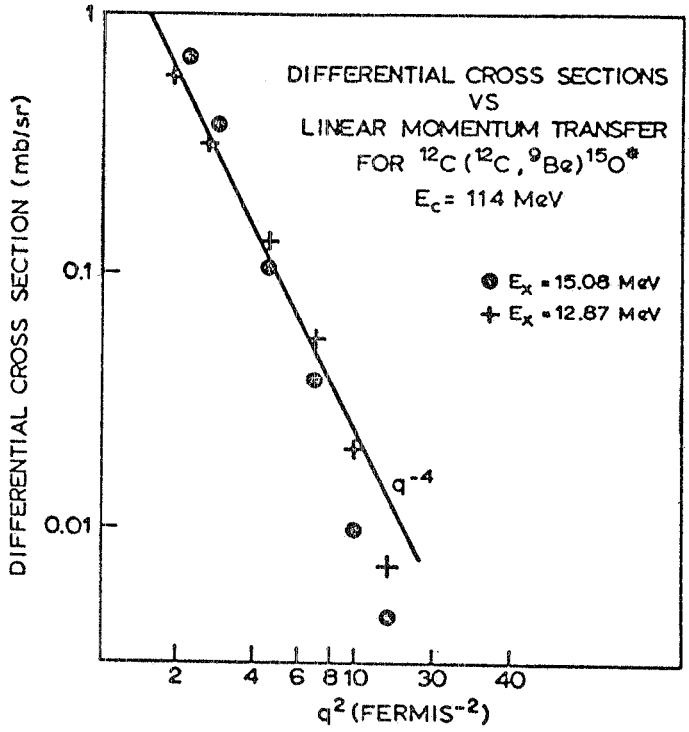

FIG. 3.11. - Differential cross-sections for the three-nucleon transfer reaction $^{12}C + ^{12}C \rightarrow ^{9}Be + ^{15}O$. The data falls uniformly on exponentially decreasing curve predicted by DWBA calculations including recoil (from ref. (3.12)).

Another plagues of DWBA method are the post-prior discrepancy, and numerical problems of dealing with many partial waves with which are associated highly oscillating functions. The post-prior asymmetry is generated by approximations within the DWBA, in particular the neglect of recoil effects, but also by the inadequacy of treating in a consistent symmetrical way the initial and final channel when approximating the residual potential. We refer here, for example, to the approximation made in the previous section where the core-core interaction V_{c_1,c_2} was approximated by the optical potential corresponding to the final channel. The 6-dimensional integral codes, which enable us to take care of recoil, remove the post-prior discrepancy, providing we do not make an approximation about the residual interaction. The plague of very many partial waves in the relative motion of heavy ions becomes very severe at high energies. The impact parameter picture suggests itself as a more proper language than the partial wave analysis.

REFERENCES. -

(3.1) - R. A. Malfliet, in Extended Seminar on Nuclear Physics, Trieste (1973).
(3.2) - N. F. Mott and H. S. W. Massey, The theory of atomic collisions (Clarendon Press, Oxford, 1965).
(3.3) - P. C. Sabatier, Nuovo Cimento 37, 1180 (1965).
(3.4) - N. K. Glendenning, Revs. Mod. Phys. 47, 659 (1975).
(3.5) - R. A. Broglia, S. Landowne, R. A. Malfliet, V. Rostokin and A. Winther, Phys. Reports 11C, 1 (1974).
(3.6) - T. W. Donnelly, J. Dubach and J. D. Walecka, Nuclear Phys. A232, 355 (1974).
(3.7) - F. D. Becchetti, P. R. Christensen, V. I. Manko and R. Y. Nickels, Nuclear Phys. A203, 1 (1973).
(3.8) - L. J. B. Goldfarb, in Oak Ridge Heavy Ion Summer Study, Oak Ridge, Tennessee (ed. S. T. Thornton) (1972).
(3.9) - P. J. A. Buttle and L. J. B. Goldfarb, Nuclear Phys. 78, 409 (1966); A176, 299 (1971).
(3.10) - H. J. Körner, G. C. Morrison, L. R. Greenwood and R. H. Siemssen, Phys. Rev. C7, 107 (1973).
(3.11) - R. L. Dodd and K. R. Greider, Phys. Rev. 146, 671 and 675 (1966).
(3.12) - D. K. Scott, in Symposium on Heavy Ion Transfer Reactions, Argonne, Illinois (1973), p. 97
(3.13) - R. M. De Vries, in Symposium on Heavy Ion Transfer Reactions, Argonne, Illinois (1973), p. 189.
(3.14) - M. Liu et al., Nuclear Phys. A143, 34 (1970); A165, 118 (1971).
(3.15) - L. R. Dodd and K. R. Greider, Phys. Rev. 180, 1187 (1969).

CHAPTER 4 - METHODS BASED ON THE EIKONAL TECHNIQUE. ELASTIC SCATTERING. -

The eikonal technique, most popularly known in its special form as the Glauber model[4.1], has been commonly applied in the high energy region for scattering of either elementary particles or nucleus on another nucleus. Particular attention of this technique to heavy ion processes has been brought in 1971 by Dar and Kirzon[4.2]. We shall come later to some details of this application, but now, staying with a more general view on the eikonal technique, not only restricted to the Glauber model, we mention several reasons which motivate the application of the eikonal approximation in studying the heavy-ion processes. They are:

a) The impact parameter representation which is the language of the eikonal scheme instead of the partial wave notion, is especially appropriate if one deals with very many partial waves arising either from the strong Coulomb field or increasing energy, or both.

b) The eikonal method is closely connected with the WKB method which in turn relates to the semiclassical method describing gross features of heavy ion processes.

c) Below the Coulomb barrier, where the Coulomb interaction plays a dominant role one can formulate the eikonal approximation in such a way that it gives the exact result for an arbitrary scattering angle and at all energies. Therefore, the association one usually has with the eikonal technique as appropriate for small scattering angle is removed in the case of dominating Coulomb field. At the Coulomb barrier and above, one must include also the strong nuclear force, and for heavy ions one can again extend the eikonal technique to an arbitrary scattering angle. The large parameter is the ratio $D\lambda^{-1}$ mentioned in the Introduction. We shall come back to this extension later in this section.

d) The eikonal technique, although an approximation, provides us often with an analytic, or almost analytic result, which can be studied from many points of view, contrary to outputs of numerical programs like that of the DWBA method, or semiclassical numerical codes.

e) It is much easier than in the standard methods to incorporate the 3-body and, in general many-body aspects of scattering of composite systems if the propagation is simplified as it is in the eikonal method.

f) Some, even crude, trials of aplying eikonal-type methods proved to be surprisingly successful. One may hope that more delicate use of the eikonal technique will not destroy the agreement, and will shed some light on the dynamics of heavy ion processes at different energies.

We shall now review several ways of applying the eikonal method to heavy ion processes and for clarity we divide our review into two big parts: one dealing with the elastic scattering (this Chapter), another one with inelastic processes (Chapter 5), and within these parts we consider separately different approaches.

4.1. - Glauber approximation. -

The eikonal approximation may be derived straightforwardly from the Schrödinger equation:

$$(\nabla^2 + k^2)\psi = 2\mu V(r)\psi \quad , \tag{4.1}$$

μ being the reduced mass.

Thus if one looks for a solution of the wave equation in the form:

$$\psi = \phi(\vec{r})\, e^{i\vec{k}\cdot\vec{r}} \quad , \tag{4.2}$$

where ϕ is a slowly varying function compared with the wave length $\lambda = k^{-1}$ (hence $\nabla^2\phi = 0$), one obtains from (4.1) :

$$\frac{\partial\phi}{\partial z} = -i\frac{\mu}{k} V\phi , \qquad \phi(-\infty) = 1 , \tag{4.3}$$

where the z-axis is chosen along the incident direction $\vec{k}$.

The solution of equation (4.3) is :

$$\psi = e^{ikz} \exp\left(-\frac{i}{v}\int_{-\infty}^{z} V(\vec{b},\zeta)\,d\zeta\right) , \tag{4.4}$$

v being the relative velocity of colliding particles.

Putting this approximate wave function in the Lippman-Schwinger equation one has for the scattering amplitude :

$$f(\vec{q}) = -\frac{\mu}{2\pi}\int d^2b\, e^{i\vec{q}_\perp\cdot\vec{b}}\int dz\, e^{iq_\parallel z}\, V(b,z)\, e^{-\frac{i}{v}\int_{-\infty}^{z} V\,d\zeta} , \tag{4.5}$$

$q_\perp$, $q_\parallel$ being the transverse and longitudinal momentum transfers, respectively.

The fact that for small-angle scattering at large momentum k one has :

$$q_\perp \cong q , \qquad q_\parallel \cong 0 , \tag{4.6}$$

allows to perform the integration over the longitudinal coordinate z. Thus one arrives to the eikonal approximation in the form given by Glauber[4.1] :

$$f(q) = \frac{ik}{2\pi}\int d^2b\, e^{i\vec{q}\cdot\vec{b}}\, \Gamma(b) , \tag{4.7}$$

where :

$$\Gamma(b) = 1 - e^{i\chi(b)} , \tag{4.8}$$

is called the profile function, and the function $\chi(b)$ is given by the integral along the direction of incident beam over the projectile-target interaction V(r) :

$$\chi(b) = -\frac{i}{v}\int_{-\infty}^{+\infty} dz\, V\left(\sqrt{b^2+z^2}\right) . \tag{4.9}$$

The function $\chi(b)$, called the eikonal (or Glauber) phase, is related to the phase-shifts δ_l in the partial-wave expansion (3.3). In fact for large k many partial waves are contributing to the scattering and one may put in (3.3) :

$$\frac{i}{2k}\sum_{l}(2l+1) \longrightarrow ik\int db\, b = \frac{ik}{2\pi}\int d^2b , \tag{4.10}$$

where the relation $kb = l + \frac{1}{2}$ was used.

Further for $l \gg 1$ and small scattering angles ($\theta \ll 1$) one may put:

$$P_l(\cos\theta) = J_o(l+\tfrac{1}{2})\theta) = J_o(qb) , \tag{4.11}$$

where $q = 2k \sin\frac{\theta}{2}$ is the c.m. momentum transfer.

Thus the partial-wave expansion (3.3), at large k and small θ, may be written exactly in the form of Eq. (4.7) with :

$$\chi(b) = 2\,\delta_l(k, l = kb) . \tag{4.12}$$

The equivalence of the Legendre sum (Eq. (3.3)) and the Fourier-Bessel integral (Eq. (4.7)) representations (in fact there is a remarkable cancellation of the remainder functions from the two approximations (4.10) and (4.11)) allows to write the eikonal approximation also in the form of the partial-wave expansion with the phase-shifts equal to half the Glauber phase (4.9).

The main advantage of the Glauber approximation (4.7 - 4.9) consists in its simplicity. Of extreme importance is that the interaction appears linearly in the eikonal phase. In the case of scattering from a composite target this leads to additivity of phase-shifts from individual constituents which is a basic assumption of the Glauber model of multiple scattering (see 4.3).

The framework of the Glauber approximation allows for a direct construction of the interaction from the phase-shifts. In fact the Glauber phase-shift (Eqs. (4.12) and (4.9)) may be written for spherical potential in the form :

$$\delta^{Gl}(b) = -\frac{1}{v}\int_b^\infty \frac{dr\, r\, V(r)}{\sqrt{r^2-b^2}} , \tag{4.13}$$

which is the integral equation for V(r) of the Abel type. Its solution is :

$$\frac{V(r)}{v} = \frac{2}{\pi}\frac{1}{r}\frac{d}{dr}\int_r^\infty \frac{db\, b\, \delta^{Gl}(b)}{\sqrt{b^2-r^2}} . \tag{4.14}$$

4.2. - Corrections to the Glauber approximation from WKB. -

It is instructive to study the relation between the Glauber approximation and the WKB method[4.3, 4.4].

Eq. (3.5) for the WKB phase-shift may be written as follows :

$$\delta^{WKB}(k,b) = k\int_{r_o}^\infty \frac{dr}{r}\left[r^2(1-\frac{V(r)}{E}) - b^2\right]^{\frac{1}{2}} - k\int_b^\infty \frac{dr}{r}(r^2-b^2)^{\frac{1}{2}} , \tag{4.15}$$

where $kb = l+\frac{1}{2}$.

Let us assume that the potential may be continued to the complex plane :

$$r \longrightarrow \varrho = r + i\,\mathrm{Im}\varrho \quad . \tag{4.16}$$

In order to proceed it is convenient to introduce the following change of variable (Sabatier transformation[4.5]):

$$t(\varrho) = \varrho\left(1 - \frac{V(\varrho)}{E}\right)^{1/2} \quad , \tag{4.17}$$

the inverse transformation being denoted $\varrho = \varrho(t)$.

With this notation Eq. (4.15) may be transformed to the form[4.4] :

$$\delta^{WKB}(k,b) = -\frac{1}{v}\int_b^\infty \frac{dt\; t\; U(t)}{\sqrt{t^2-b^2}} = -\frac{1}{v}\int_0^\infty dz\; U\left(\sqrt{b^2+z^2}\right) \quad , \tag{4.18}$$

where U(t), called the quasi-potential, is defined as follows :

$$U(t) = vk \ln\frac{\varrho(t)}{t} \quad . \tag{4.19}$$

Thus the WKB phase-shift assumes the simple appearance of the Glauber phase-shift (4.13), the essential difference being the replacement of the exact potential by a quasi-potential.

The relation between the potential and quasi-potential may be written in the following compact forms :

$$U(t) = -E \ln\left[1 - \frac{V(\varrho)}{E}\right] \quad ,$$

or

$$V(\varrho) = E\left[1 - \exp\left(-\frac{U(t)}{E}\right)\right] \quad , \tag{4.20}$$

where

$$\varrho(t) = t\exp\left(\frac{U(t)}{2E}\right) \quad , \qquad E = \frac{k^2}{2\mu} \quad .$$

The Glauber approximation may be considered as the high-energy limit of the WKB method. If $V/E \ll 1$, the quasi-potential is simply the potential, and the WKB and Glauber phase-shifts coincide.

Expanding Eq. (4.18) in a Taylor series about $1/k^2=0$, one obtains with the aid of Eq. (4.20)[4.3] :

$$\delta^{WKB}(k,b) = \delta^{Gl} + \delta^{(1)} + \delta^{(2)} + \cdots$$

where :

$$\delta^{Gl} = -\frac{1}{v}\int_0^\infty dz\; V\left(\sqrt{b^2+z^2}\right) ,$$

$$\delta^{(1)} = -\frac{1}{v^2 k}\int_0^\infty dz\; \frac{d}{dr^2}\left[r^2 V^2(r)\right] , \tag{4.21}$$

$$\delta^{(2)} = -\frac{2}{3v^3k^2}\int_0^\infty dz\left(\frac{d}{dr^2}\right)^2\left[r^4V^3(r)\right] . \qquad (4.21)$$

It should be observed that the corrections to the simple Glauber result, because of the derivatives of the potential, are most important at the nuclear surface.

The relation of the Glauber approximation to the WKB method is illustrated in Fig. 4.1 on the example of elastic scattering ^{16}O-^{60}Ni for a series of c.m. energies[4.3].

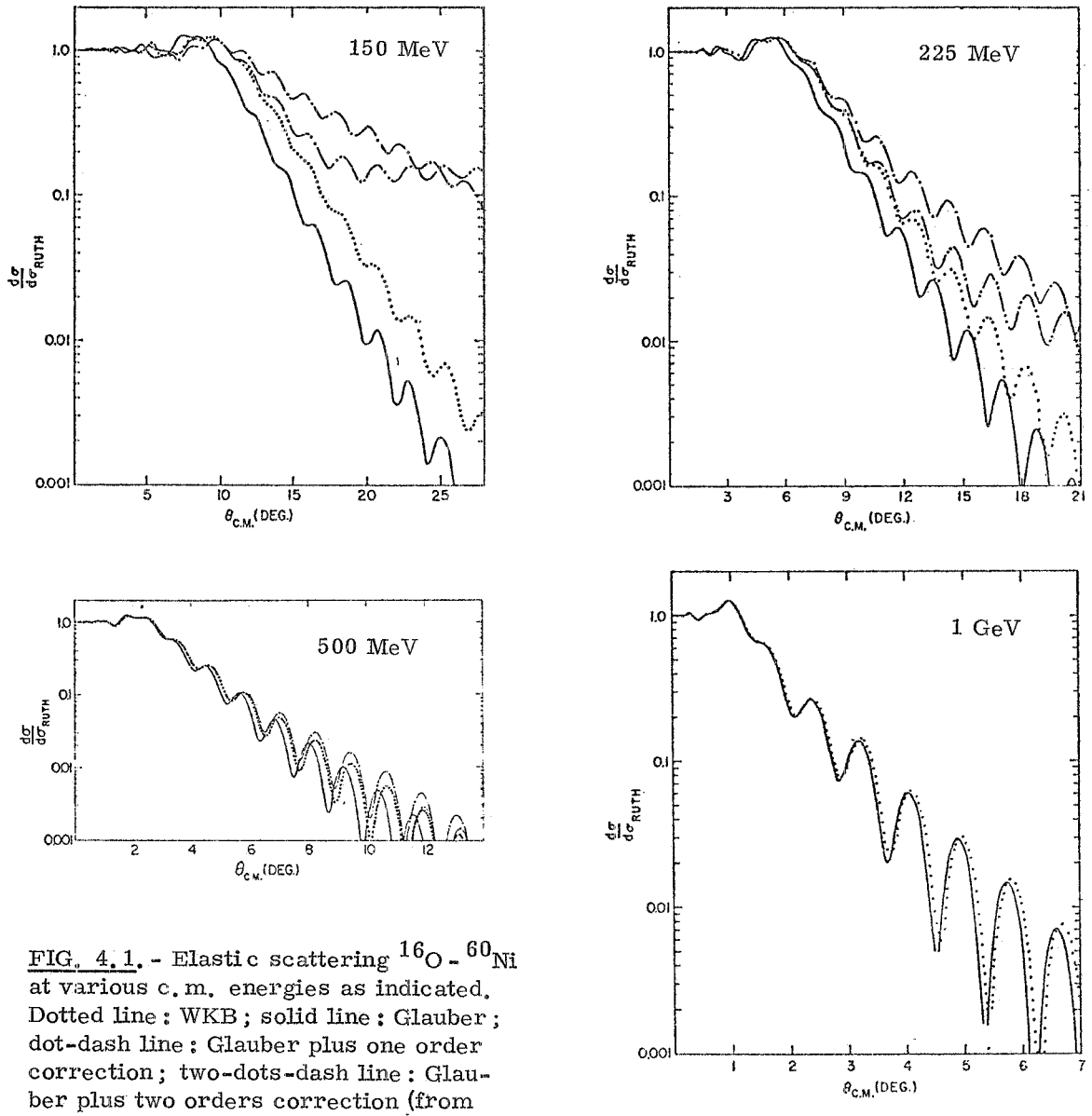

FIG. 4.1. - Elastic scattering ^{16}O - ^{60}Ni at various c.m. energies as indicated. Dotted line: WKB; solid line: Glauber; dot-dash line: Glauber plus one order correction; two-dots-dash line: Glauber plus two orders correction (from ref. (4.7). In all cases the same optical model parameters as for Fig.3.5 are used, although the "point-sphere" Coulomb potential in Eq. (3.15) is replaced by the "sphere-sphere" Coulomb potential.

Here the Glauber and WKB phase-shifts are used in the partial-wave expansion (3.3). The full WKB result may be considered as a point of reference since, as explained in Fig. 3.5, it should coincide with the exact optical-model calculation. In general the Glauber approximation reproduces the qualitative shape of the curve quite well although it is sfifted toward smaller angles and smaller cross-sections. With increasing energy the agreement between the Glauber and WKB results becomes more and more satisfactory. The WKB corrections greatly improve the positions of the maxima and minima in the curve, but the magnitude of the cross section, although in excellent agreement at small angles, can be in serious error at large angles.

If the phase-shifts are known Eq. (4.18) may be viewed as an Abel integral equation and solved for the quasi-potential U(t) - compare Eq. (4.14). Then the potential V(r) can be constructed proceeding as follows[4.4]: Given U(t) one can determine from (4.20) $V(\varrho)$ and ϱ for any value of the complex variable $t = t_R + i t_I$. The true potential V(r) is to be computed along the path in the complex t plane given by $\mathrm{Re}\,\varrho = r$, $\mathrm{Im}\,\varrho = 0$. This condition provides, together with Eq. (4.20), unequivocal relations $t_I = t_I(t_R)$, $r = r(t_R)$, and allows to compute V(r).

The potential constructed in such a way is an approximate solution to the inverse scattering problem within the framework of the WKB approximation. It consequently has a wider range of validity than the Glauber approximation (Eq. (4.14)) to which it reduces in the high-energy limit. The relation between the WKB and Glauber potentials has been studied by Kujawski[4.4]. He assumed a specific and realistic form of the phase-shifts and treated the resulting cross-sections, given by Eq. (3.3), as "data". The equivalent optical potential was constructed following the procedure described above - the WKB and Glauber potentials for α-^{42}Ca at 42 and 166 MeV are shown in Fig. 4.2. The validity of these potentials was then investigated by exactly solving the Schrödinger equation and comparing the resulting angular distributions with the corresponding "data" - see Fig. 4.3. We see that the potentials obtained in the WKB approximation yield results in good agreement with the "data" up to 40°-50°. The range of validity of the Glauber approximation is more limited. At larger angles both the approximations become unreliable.

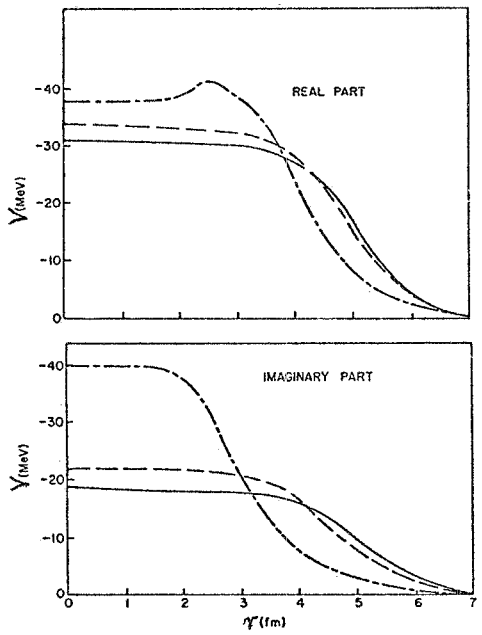

FIG. 4.2. - The real and imaginary parts of the calculated WKB[4.4] (dash-dot line for α-^{42}C at 42 MeV, dashed line for α-^{42}C at 166 MeV), and Glauber (solid line) optical potentials. The nuclear phase-shift function was assumed in the form:

$$\delta(b) = -\frac{U_R + iU_I}{v}\int_0^{\infty} dz \left[1+\exp\left(\frac{r-R}{a}\right)\right]^{-1}.$$

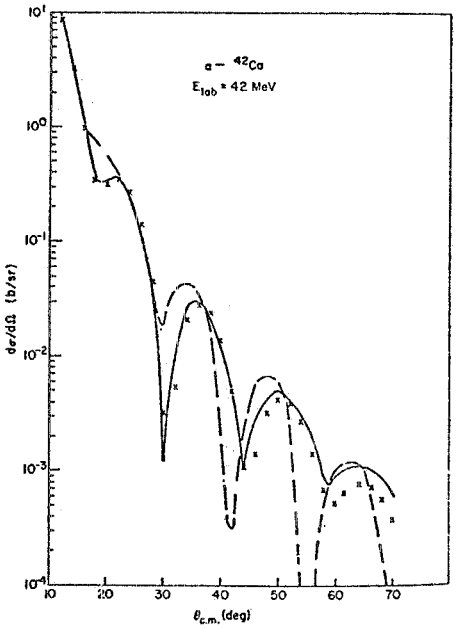

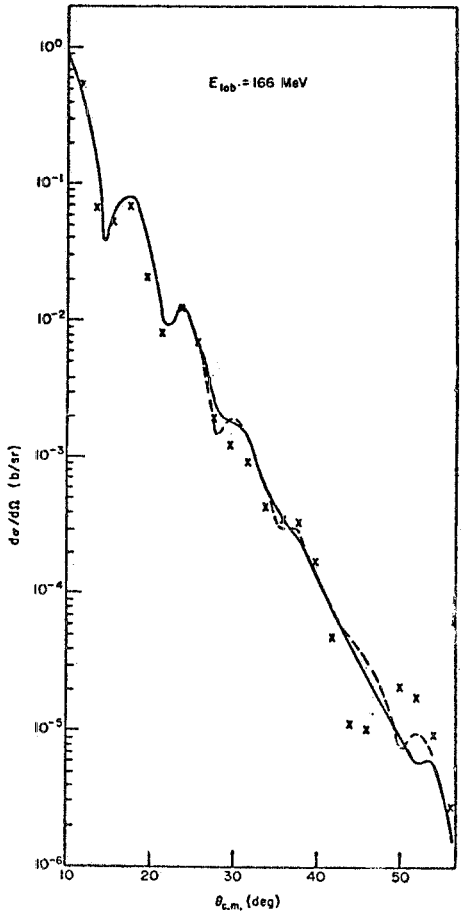

FIG. 4.3. - The elastic differential cross-sections for the scattering of 42 MeV and 166 MeV α particles by ^{42}Ca[12]. Solid line: solution for the WKB potential; dotted line: solution for the Glauber potential. The "data" points are denoted by crosses.

4.3. - Glauber model of multiple scattering. -

Let us consider collision of two nuclei with A and B nucleons, respectively - see Fig. 4.4.

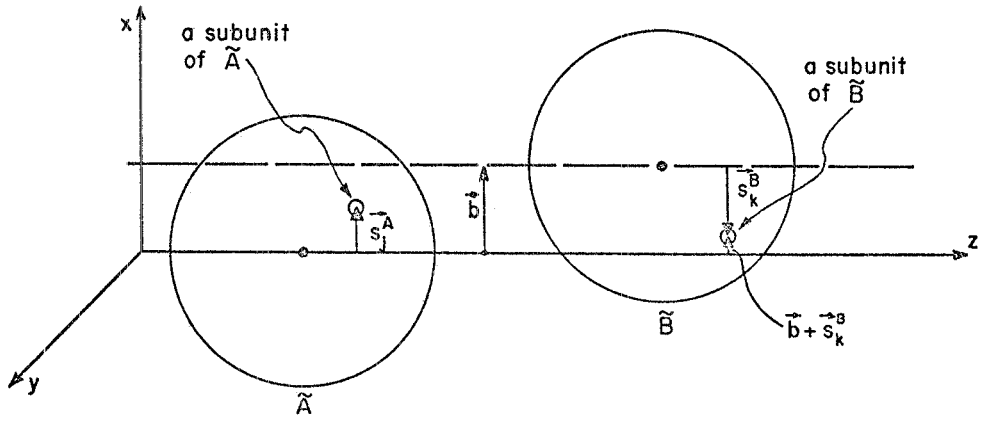

FIG. 4.4. - The geometry of collision A + B.

We assume that the total interaction between the incident and target nuclei is a sum of individual nucleon-nucleon (one from A, the other from B) interactions. Let us calculate now the phase-shift for scattering of the two nuclei in the framework of Glauber approximation - Eq. (4. 9). The fact that the interaction appears linearly in the Glauber phase leads to simple additivity of the individual nucleon-nucleon phase-shifts :

$$\chi(b) = \sum_{j=1}^{A} \sum_{k=1}^{B} \chi_{jk}(\vec{b} - \vec{s}_j^A + \vec{s}_k^B) \quad . \tag{4. 22}$$

The additivity of phase-shifts leads in turn to the following composition law for the profile function (4. 8) :

$$\Gamma(b) = 1 - \prod_{j=1}^{A} \prod_{k=1}^{B} e^{i\chi_{jk}(\vec{b}-\vec{s}_j^A+\vec{s}_k^B)} = 1 - \prod_{j=1}^{A} \prod_{k=1}^{B} \left[1 - \gamma_{jk}(\vec{b} - \vec{s}_j^A + \vec{s}_k^B)\right] , \tag{4. 23}$$

where we have introduced the profiles for nucleon-nucleon collisions through the definition analogous to Eq. (4. 8). The elementary profiles $\gamma_{jk}(\vec{b} - \vec{s}_j^A + \vec{s}_k^B)$ may be expressed, by inverting the Fourier-Bessel transformation, through the nucleon-nucleon elastic scattering amplitudes $f_{jk}(q)$, which are to be taken from the experiment with free particles.

In writing the above expressions we keep the projectile and target nucleons in the space positions given by the vectors $\vec{s}_j^A$, $\vec{s}_k^B$, respectively, in the plane of impact parameters, i. e. the plane perpendicular to the incident beam - see Fig. 4. 4. Hence we treat the nucleons as they were frozen in a certain geometrical configuration. This assumption is justified if the time of collision is very short so the projectile is gone before any rearrangement it induces in the target can take place. Obviously one should then average over all possible internal configurations by sandwiching the operator of transition between the initial and final nuclear states.

Thus the final expression for the amplitude of transition in the Glauber model may be written as follows :

$$F_{ji}(q) = \frac{ik}{2\pi} \int d^2b \, e^{i\vec{q}\cdot\vec{b}} \left\langle f_A f_B \left| 1 - \prod_{j=1}^{A} \prod_{k=1}^{B} \left[1 - \gamma_{jk}(\vec{b} - \vec{s}_j^A + \vec{s}_k^B)\right] \right| i_A i_B \right\rangle , \tag{4. 24}$$

i_A, i_B, f_A, f_B being the initial and final wave functions of the two nuclei. Eq. (4. 24) describes elastic as well as inelastic scattering. The inelasticity is meant here in nuclear sense, i. e. the nuclei may become excited or even broken up, but their constituents do not change in any essential way.

To summarize let us stress the main points underlying the Glauber model[4. 1] :

a) High energy small angle scattering (eikonal approximation) ;
b) Additivity of phase-shifts ;
c) Expression of individual phase-shifts (profiles) by means of elementary phenomenological elastic amplitudes ;
d) Averaging of the operator of scattering over the nuclear states.

If we multiply out the AB factors in the expression (4. 23) we obtain the sum of terms with different powers of elementary profiles. This sum is finite (extending up to the AB-th order) and has alternative signs. The individual terms of this series are referred to as the contributions from single, double, triple, etc. scattering.

The different orders of scattering interfere with each other in a destructive way. The most important results of this interference are the diffractive structure (maxima and minima)

of elastic angular distributions, and the defect effect in the total cross-section.

Let us discuss in more detail the elastic scattering of heavy ions. We choose the matter densities of nuclei A, B in the form of independent particle model (IPM):

$$\left| i_A \right|^2 = \left| f_A \right|^2 = \prod_{j=1}^{A} \varrho_A(r_j^A) ,$$
$$\left| i_B \right|^2 = \left| f_B \right|^2 = \prod_{k=1}^{B} \varrho_B(r_k^B) . \qquad (4.25)$$

It was shown by Czyz and Maximon[4.6] that for large A and B the expectation value of the profile operator (4.23) may be written then in the form:

$$\langle i_A i_B | \Gamma(b; \vec{s}_j^A, \vec{s}_k^B) | i_A i_B \rangle = 1 - (1 - \langle \gamma_{AB} \rangle)^{AB} , \qquad (4.26)$$

where:

$$\langle \gamma_{AB} \rangle = \int d^2 s_A \, d^2 s_B \, \varrho_A^{(2)}(s_A) \gamma(\vec{b} - \vec{s}_A + \vec{s}_B) \gamma_B^{(2)}(s_B) ,$$
$$\varrho_A^{(2)}(s_A) = \int dz \, \varrho_A(\vec{s}_A, z) , \qquad (4.27)$$
$$\varrho_B^{(2)}(s_B) = \int dz \, \varrho_B(\vec{s}_B, z) .$$

Thus for heavy ion elastic scattering the Glauber model gives in the framework of IPM (Eq. (4.25)) the following expression:

$$F(q) = \frac{ik}{2\pi} \int d^2 b \, e^{i\vec{q}\cdot\vec{b}} \left[1 - (1 - \langle \gamma_{AB} \rangle)^{AB} \right] \cong \frac{ik}{2\pi} \int d^2 b \, e^{i\vec{q}\cdot\vec{b}} \left[1 - e^{-AB \langle \gamma_{AB} \rangle} \right] , \qquad (4.28)$$

where in the second equation an exponentiation, justified for large A and B, has been carried out.

Since the amplitude assumes the simple appearance of the Glauber approximation for scattering in a potential field, the limit of large A and B is usually called the optical limit. The optical limit of the Glauber model provides a bridge between the phenomenological approach of the optical model and the microscopic description of multiple scattering. In fact, the optical phase-shift and the equivalent optical potential can be expressed in terms of the microscopic quantities: nuclear densities and profiles of the elementary interaction. From Eqs. (4.8), (4.9) and (4.28) one has:

$$i\chi(b) = - AB \langle \gamma_{AB} \rangle ,$$
$$V(b, z) = -iv AB \int d^2 s_A \int d^3 r_B \, \varrho_A(r_A) \gamma(\vec{b} - \vec{s}_A + \vec{s}_B) \varrho_B(r_B) . \qquad (4.29)$$

These expressions may be simplified by noting that the elementary profile (being of size of the nucleon) is a very sharply peaked function compared to nuclear density. Thus to a good approximation one may put:

$$\gamma(\vec{b}-\vec{s}) = \frac{\sigma^{NN}(1-i\alpha)}{2}\,\delta^{(2)}(\vec{b}-\vec{s}) \,, \tag{4.30}$$

where the coefficient has been established from the optical theorem, σ^{NN} being the total nucleon-nucleon cross-section and α - the ratio of the real to imaginary part for the forward elementary amplitude.

From Eqs. (4.29) and (4.30) one obtains :

$$\begin{aligned} i\chi(b) &= -\frac{\sigma^{NN}(1-i\alpha)}{2} AB\int d^2 s_B\, \varrho_A^{(2)}(\vec{b}-\vec{s}_B)\,\varrho_B^{(2)}(s_B) \,, \\ V(r) &= -iv\frac{\sigma^{NN}(1-i\alpha)}{2} AB\int d^3 r_B\, \varrho_A(\vec{r}-\vec{r}_B)\,\varrho_B(r_B) \,. \end{aligned} \tag{4.31}$$

Thus the equivalent optical potential is proportional to the convolution of densities of two colliding nuclei.

The Glauber model has been extensively applied to the heavy ion elastic scattering by Dar and Kirzon[4.2]. They write the scattering amplitude in the form of the partial wave expansion. The phase-shifts contain the Coulomb part, corresponding to the interaction between two point charges, and the nuclear part which is put equal to half (see Eq. (4.12)) the Glauber phase $\chi(b)$, as given in Eq. (4.31). The only parameters needed in the calculations are thus σ^{NN}, α and the parameters of the nuclear density distribution. A systematic search with a best-fit program has been done to find the "best-values" for these parameters, both for a Saxon-Woods density and for a Gaussian density. The comparison between the theoretical curves and the experimental data, for a wide range of masses and energies, is presented in Figs. 4.5 - 4.10.

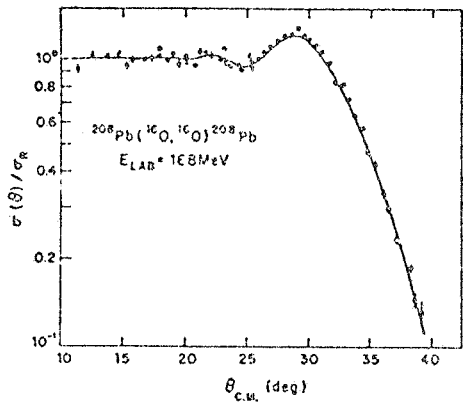

FIG. 4.5. - Elastic scattering of ^{16}O on ^{208}Pb (Ref. (4.2)) at 158 MeV ; equivalent energy per nucleon is 4 MeV, σ^{NN}_{exp} = 2400, σ^{NN}_{th} = 2340 mb.

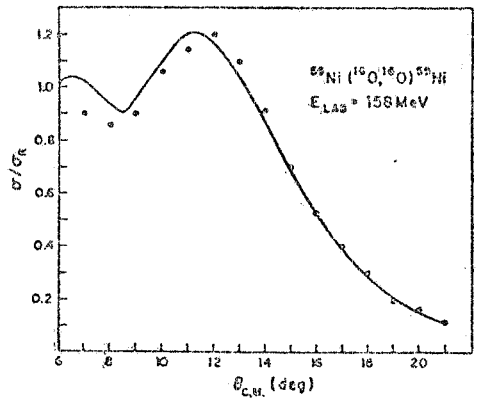

FIG. 4.6. - Elastic scattering of ^{16}O on ^{59}Ni (Ref. (4.2)) at 158 MeV ; equivalent energy per nucleon is 7.2 MeV, σ^{NN}_{exp} = 1300, σ^{NN}_{th} = 1500 mb.

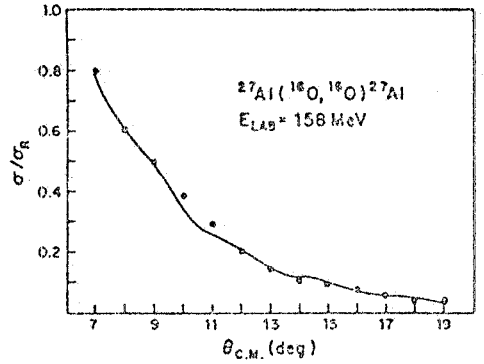

FIG. 4.7. - Elastic scattering of ^{16}O on ^{27}Al (Ref. (4.2)) at 158 MeV; equivalent energy per nucleon is 8.4 MeV, σ_{exp}^{NN} = 1200, σ_{th}^{NN} = 1290 mb.

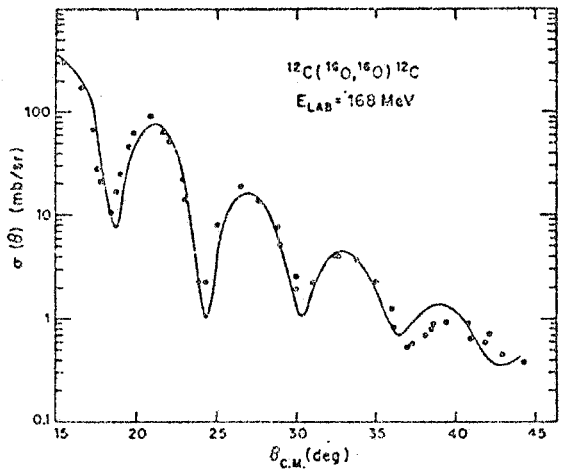

FIG. 4.8. - Elastic scattering of ^{16}O on ^{12}C (Ref. (4.2)) at 168 MeV; equivalent energy per nucleon is 9.8 MeV, σ_{exp}^{NN} = 1050, σ_{th}^{NN} = 760 mb.

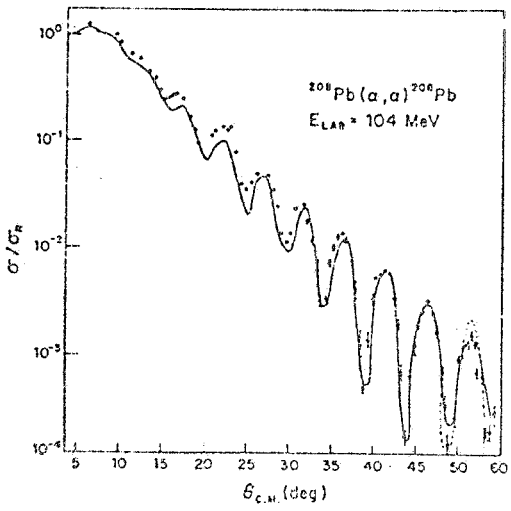

FIG. 4.9. - Elastic scattering of α-particles on ^{208}Pb (Ref. (4.2)) at 104 MeV; equivalent energy per nucleon is 18 MeV, σ_{exp}^{NN} = 530, σ_{th}^{NN} = 500 mb (dashed line) and 300 mb (full line).

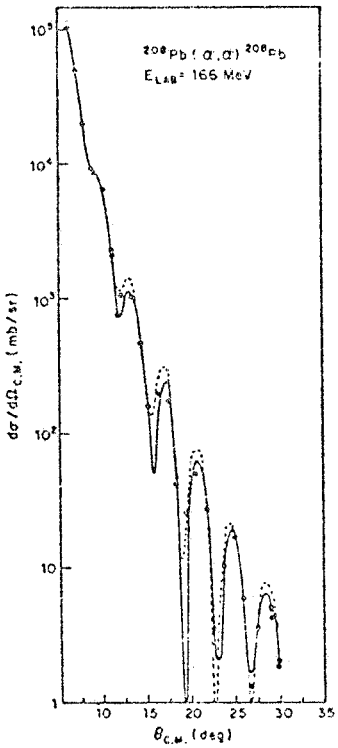

FIG. 4.10. - Elastic scattering of α-particles on ^{208}Pb (Ref. (4.2)) at 166 MeV; equivalent energy per nucleon is 34 MeV, σ_{exp}^{NN} = 300, σ_{th}^{NN} = 250 mb (dashed line) and 224 mb (full line).

It appears that the angular distributions in Figs. 4.5 - 4.10 are well fitted with σ^{NN}, which is in significant agreement with the experimental nucleon total cross-section. The parameter α is, in general, higher than its experimental value. It may, however, be pointed out that the corrections of higher powers of the nuclear density, which should be added to the phase shift $\chi(b)$ in Eq. (4.31), can be regarded as an effective correction to σ^{NN} and α.

As for the nuclear parameters, in the case of Saxon-Woods densities the fitted values of r_o ($R = r_o A^{1/3}$) fall into the range 1.0 - 1.2 fm (the lower limit is in agreement with electron scattering data), and the fitted values for the diffuseness a take the values 0.5 - 0.65 fm.

Despite of various kinds of ambiguities in fixing the parameters, the comparison shown in Figs. 4.5 - 4.10 demonstrates that the elastic scattering of heavy ions can be well reproduced (the greater energy the better) be means of the nuclear density and the free nucleon-nucleon total cross-section.

4.4. - Exact solution and an eikonal correction. -

The eikonal technique, which is simpler than the WKB method, may be extended both to larger angles and lower energies if it is combined with some known analytic solution, so that the eikonal method is used only for evaluating corrections arrising from a small difference between the actual potential and the solvable one. Such method was developed by Bartnik, Iwinski and one of the present authors[4.7] to deal with the screened Coulomb potential. We present this method on the case of the Coulomb potential, where it was tested, and indicate its extension to the case of a sum of nuclear and Coulomb potential. The last topic is currently investigated numerically.

For a Coulomb point-like potential $V_c(r) = \frac{Z_p Z_t e^2}{r}$ we have :

$$\left(-\frac{\hbar^2}{2}\nabla^2 + V_c - E\right)\psi_c = 0 ,$$

$$\psi_c = \sqrt{\frac{\mu}{k}}\,\Gamma(1+i\eta)\,e^{-\frac{\pi}{2}\eta}\,e^{i\vec{k}\cdot\vec{r}}\,{}_1F_1(-i\eta;1;ik(r-z)) , \tag{4.32}$$

with :

$$k = (2\mu E)^{1/2} , \qquad \eta = Z_p Z_t e^2 \mu (\hbar k)^{-1} ,$$

μ - being the reduced mass of two ions.

For $V \neq V_c$, e.g. for a screened Coulomb field we write the Schrödinger equation in the form:

$$\left[-\frac{\hbar^2}{2\mu}\nabla^2 + V_c + (V - V_c) - E\right]\psi = 0 , \tag{4.33}$$

and look for its solution in the form:

$$\psi = f \exp(i\vec{k}\cdot\vec{r}) . \tag{4.34}$$

So, f must satisfy the equation:

$$\left[\nabla^2 + 2i\vec{k}\cdot\vec{\nabla} - 2\mu V_c - 2\mu(V - V_c)\right] f = 0 , \tag{4.35}$$

and appropriate boundary conditions.

The essential point in the method of Bartnik et al.[4.7] is to replace Eq. (4.35) by such 1-st order differential equation which by definition will reproduce the known result given by Eq. (4.32) at all scattering angles and at all energies. It can be formally achieved by introducing a function f_c defined by :

$$\psi_c \equiv f_c \exp(i\vec{k}\cdot\vec{r}) \ , \tag{4.36}$$

and another function A which must satisfy the equation :

$$(2i\vec{k}\cdot\vec{\nabla} - 2\mu V_c + A) f_c = 0 \ . \tag{4.37}$$

The same A is then used in an equation which replaces Eq. (4.35). It is :

$$\left[2i\vec{k}\cdot\vec{\nabla} - 2\mu V_c + A - 2\mu (V - V_c)\right] f = 0 \ , \tag{4.38}$$

and in contrast to Eq. (4.35) it is very easy to solve. The solution of Eq. (4.38) is :

$$f = f_c f_1 \ , \tag{4.39}$$

where f_1 satisfies the equation:

$$i\vec{k}\cdot\vec{\nabla} f_1 = \mu (V - V_c) f_1 \ , \tag{4.40}$$

thus it is simply given as :

$$f_1 \sim \exp\left[-i \frac{\mu}{k} \int (V - V_c)\, dz\right] \ , \tag{4.41}$$

with the z-axis along the direction $\vec{k}$. It was found in Ref. (4.7) that the solution of the whole problem written as $\psi = f_c f_1 \exp(i\vec{k}\cdot\vec{r})$ satisfies the exact 2-nd order differential equation (4.35) with an accuracy better than 3%, practically in the whole configuration space.

To apply the above method for evaluating differential cross-section for the elastic scattering of heavy ions one must extend this method to include both the nuclear and Coulomb potential. For two heavy ions the exact potential is taken as the square well in the inner region and the point-like Coulomb potential in the outer region. We have :

$$V_{exact} = \begin{cases} -V_o & \text{for} \quad r < a \\ V_c & \text{for} \quad r \geq a \ , \end{cases} \tag{4.42}$$

where a is a characteristic distance.

The Schrödinger equation is solved by taking the analytic solutions corresponding to the square well and to V_c, and by adjusting numerically constants, requiring the standard continuity condition at $r = a$. This should be done without using the partial wave expansion. Having explicity such ψ_{exact} we define f_{exact} by :

$$\psi_{exact} = f_{exact} \exp(i\vec{k}\cdot\vec{r}) \ , \tag{4.43}$$

and find the wave function for the actual potential :

$$V = V_N + V_c \ , \tag{4.44}$$

in the following form :

$$\psi = f_{exact} \exp\left[i\vec{k}\cdot\vec{r} - i\frac{\mu}{k} \int_{-\infty}^{z} (V_N + V_c - V_{exact})\, d\zeta \right] \ . \tag{4.45}$$

The scattering amplitude is then calculated from the t-matrix element found by a numerical integration of ψ with V and a plane wave :

$$\begin{aligned} \langle k'|t|k\rangle &= \langle \vec{k}'|V_N+V_c|\psi\rangle = (2\pi)^{-3}\int d^3r \left[V_N(r)+V_c(r)\right] f_{exact} \ x \\ & x \ \exp\left[i(\vec{k}-\vec{k}')\cdot\vec{r} - i\frac{\mu}{k}\int_{-\infty}^{z} (V_N+V_c-V_{exact})\, d\zeta \right] = \\ &= (2\pi)^{-2}\int dz\, b\, db\, J_o(b|\vec{k}-\vec{k}'|_\perp)\left[V_N(\sqrt{b^2+z^2})+V_c(\sqrt{b^2+z^2})\right] f_{exact} \ x \\ & x \ \exp\left[i(k_{||}-k'_{||})z - i\frac{\mu}{k}\int_{-\infty}^{z} (V_N+V_c-V_{exact})\, d\zeta \right] \ , \end{aligned} \tag{4.46}$$

where $(\vec{k}-\vec{k}')_\perp$, and $k_{||} - k'_{||}$ denote the components of momentum transfer, perpendicular and parallel to the chosen eikonal direction, respectively.

There are three numerical integrations needed in Eq. (4.46) and the hope is that they will be less time consuming and more stable than an explicit numerical solving of the Schrödinger equation for each partial wave. The advantage of our method should manifest itself especially at medium and high energy where the number of partial waves is very large indeed.

REFERENCES. -

(4.1) - R. J. Glauber, in Lectures in Theoretical Physics (ed. W. E. Brittin) (Interscience Publ., 1959), Vol. I, p. 315; in High Energy Physics and Nuclear Structure (ed. S. Devons) (Plenum Press, 1970), p. 207.
(4.2) - A. Dar and Z. Kirzon, Phys. Letters 37B, 166 (1971); Nuclear Phys. A237, 319 (1975).
(4.3) - T. W. Donnelly, J. Dubach and J. D. Walecka, Nuclear Phys. A232, 355 (1974).
(4.4) - E. Kujawski, Phys. Rev. C6, 709 (1972).
(4.5) - P. C. Sabatier, Nuovo Cimento 37, 1180 (1965).
(4.6) - W. Czyz and L. C. Maximon, Ann. Phys. 52, 59 (1969).
(4.7) - E. A. Bartnik, Z. R. Iwinski and J. M. Namysłowski, Phys. Letters 53A, 5 (1975); Phys. Rev. A12, 1785 (1975).

CHAPTER 5 - EIKONAL TECHNIQUE FOR INELASTIC PROCESSES. -

5.1. - Coulomb excitation. -

The simplest inelastic process is the Coulomb excitation. Only the energy is transferred to the target in this process, and the interaction potential responsible for excitation is the well known Coulomb potential. There exist programs which allow for the numerical evaluation of Coulomb excitation cross section within either classical, or semiclassical or quantal scheme based on the DWBA method. Although the agreement of results evaluated from these programs and the experimental data is satisfactory, the numerical routines are vary lengthy and preclude any inside into the formulae. Goldfarb and one of the present authors[5.1] applied the eikonal technique to get analytic expression for Coulomb excitation, and in this way to gain some understanding of its dynamics. In particular they looked at the role played by the nuclear moments in the expression for the transition matrix element.

Three points must be noted before discussing the final result:

a) Most of the data for Coulomb excitation process is concentrated at large scattering angles, because in the forward direction the Rutherford scattering dominates the yield;
b) Coulomb excitation process is an inelastic one, and it may be associated with some features of an off-energy shell t-matrix element, with a shift of energy corresponding to the excitation energy;
c) For energies below the Coulomb barrier the DWBA scheme is quite adequate, and both the Coulomb distorted eigenfunctions and the interaction Hamiltonian causing transition are well known.

Because of the first point one must deal with such an eikonal scheme which would give good result for large scattering angles. Luckily enough in the case of a point-like Coulomb potential, approximated as a limiting case of the Yukawa potential :

$$V_c(r) = \lim_{\beta \to 0} \exp(-\beta r) \frac{Z_p Z_t e^2}{r} \quad , \tag{5.1}$$

one can show that choosing our eikonal direction along the mean value of the initial and final relative momentum $\vec{\varkappa} = 1/2\,(\vec{k}_i + \vec{k}_f)$, and defining the eikonal propagator with a pole depending in a special way on the scattering angle, namely :

$$\tilde{G}_o = m^{-1}(2mE)^{1/2}\left[p_{\parallel} - (2mE)^{1/2}\cos\frac{\theta}{2} - i\varepsilon\right]^{-1} \quad , \tag{5.2}$$

it holds that the eikonal t-matrix t defined as :

$$\tilde{t} = -(2\pi)^2 m \left\langle \vec{k}_f \middle| V_c - V_c \tilde{G}_o V_c + V_c \tilde{G}_o V_c \tilde{G}_o V_c - \cdots \middle| \vec{k}_i \right\rangle \tag{5.3}$$

considered on the energy shell, coincides with the exact on-shell scattering t-matrix. It is most important that the agreement holds for an arbitrary scattering angle and an arbitrary energy.

Coming to the 2-nd point we note that there exists an exact expression for the half-off-shell Coulomb t-matrix. Considering the case $|\vec{k}_f| < |\vec{k}_i|$ i.e. the one interesting for Coulomb excitation, we write the result of Ford[5.2] :

$$t^{\text{half-shell}}_{\text{exact}} = -2(2\pi\eta_i)^{1/2} k_i\eta_i \left|\vec{k}_i - \vec{k}_f\right|^{-2} \left\{(k_i^2 - k_f^2)\left|\vec{k}_i - \vec{k}_f\right|^{-2}\right\}^{i\eta_i} \quad x$$

$$x \quad \exp\left[\frac{i\pi}{4} + i\eta_i \ln(\eta_i e^{-1})\right] \quad , \tag{5.4}$$

where η_i is the Sommerfeld parameter with $k = |\vec{k}_i|$.

The exact half-off-shell Coulomb t-matrix may be reproduced in the eikonal scheme if we choose a new eikonal direction and also consider heavy ions, so that η_i, $\eta_f >> 1$. For large values of the Sommerfeld parameter one can analytically evaluate a first derivative with respect to the charge of target, of the half-off-shell eikonal t-matrix. Denoting by ϱ the ratio of the magnitude of the parallel component of momentum transfer to the perpendicular component :

$$\varrho = \left|k_{f_\parallel} - k_{i_\parallel}\right| \cdot \left|\vec{k}_{f_\perp} - \vec{k}_{i_\perp}\right|^{-1} \quad , \tag{5.5}$$

where $\parallel$ is along the eikonal direction, one can find :

$$\frac{\partial}{\partial z_t} t^{\text{half-shell}}_{\text{eikonal}} = 2ik_i\eta_i Z_t^{-1}(\pi\eta_i)^{1/2} \left|\vec{k}_i - \vec{k}_f\right|^{-2-2i\eta_i} (\varrho^{-1/2} + i\varrho^{1/2}) \quad x$$

$$x \quad \exp\left[-2\eta_i \tan^{-1}\varrho + 2i\eta_i \ln(2\eta_i e^{-1})\right] \quad .$$

The direction $\parallel$, i.e. the magnitude of ϱ , is fixed by the requirement :

$$\left|\frac{\partial}{\partial z_t} t^{\text{half-shell}}_{\text{eikonal}}\right| = \left|\frac{\partial}{\partial z_t} t^{\text{half-shell}}_{\text{exact}}\right| \quad . \tag{5.6}$$

It gives ϱ as the solution of the following transcendental equation :

$$(1+\varrho^2)\varrho^{-1} \exp(-4\eta_i \tan^{-1}\varrho) = 2\eta_i^2 \ln^2\left[\eta_i(k_i^2 - k_f^2)\left|\vec{k}_i - \vec{k}_f\right|^{-2}\right] \quad . \tag{5.7}$$

Finally, we come to the 3-rd point and consider the Coulomb excitation process within DWBA scheme. Let us denote the relative position variable between a point-like projectile and the centre of target by $\vec{r}$ and a variable denoting position of distributed charge in an extended target by $\vec{r}_p$. Then, the interaction Hamiltonian describing the relative motion of the projectile in the field of charged target nucleus is :

$$H = Z_t e^2 \left|\vec{r}_p - \vec{r}\right|^{-1} = Z_t e^2 r^{-1} + Z_t e^2 \left[\left|\vec{r}_p - \vec{r}\right|^{-1} - r^{-1}\right] \quad . \tag{5.8}$$

This splitting of the Hamiltonian into the first part which generates the distorted wave eigen-

functions and into the residual part, depending explicitly on r_p is characteristic of the DWBA procedure.

The Coulomb excitation transition amplitude is given by the matrix element evaluated between the target's nuclear states of a Coulomb distorted amplitude. More explicitly, we have :

$$T_{f_i}^{\text{Coulomb excitation}} = \left\langle \varphi_f(\vec{r}_p) \left| t_{f_i}^{\text{DWBA}}(\vec{r}_p) \right| \varphi_i(\vec{r}_p) \right\rangle , \tag{5.9}$$

where $|\varphi_i(\vec{r}_p)\rangle$, $|\varphi_f(\vec{r}_p)\rangle$ are the target states, and :

$$t_{f_i}^{\text{DWBA}}(\vec{r}_p) = -(2\pi)^2 m \left\langle \chi_c(\vec{k}_f, \vec{r}) \left| Z_t e^2 \left| \vec{r}_p - \vec{r} \right|^{-1} - Z_t e^2 r^{-1} \right| \chi_c(\vec{k}_i, \vec{r}) \right\rangle \tag{5.10}$$

with $\chi_c(\vec{k}_f, \vec{r})$ and $\chi_c(\vec{k}_i, \vec{r})$ denoting the Coulomb distorted waves.

We write :

$$V_{\vec{r}_p} = Z_t e^2 \left| \vec{r}_p - \vec{r} \right|^{-1} , \qquad V = Z_t e^2 r^{-1} , \tag{5.11}$$

and evaluate $t_{f_i}^{\text{DWBA}}(\vec{r}_p)$ in the eikonal framework splitting it into four parts :

$$t_{f_i}^{\text{DWBA}}(\vec{r}_p) = t^{(1)}(\vec{r}_p) - t^{(1)} + t^{(2)}(\vec{r}_p) - t^{(2)} , \tag{5.12}$$

where :

$$t^{(1)}(\vec{r}_p) = -(2\pi)^2 m \left\langle \vec{k}_f \left| V_{\vec{r}_p} (1 - \tilde{G}_o^{(i)} V + \tilde{G}_o^{(i)} V \tilde{G}_o^{(i)} V - \ldots.) \right| \vec{k}_i \right\rangle$$

$$t^{(1)} = -(2\pi)^2 m \left\langle \vec{k}_f \left| V (1 - \tilde{G}_o^{(i)} V + \tilde{G}_o^{(i)} V \tilde{G}_o^{(i)} V - \ldots.) \right| \vec{k}_i \right\rangle$$

$$t^{(2)}(\vec{r}_p) = -(2\pi)^2 m \left\langle \vec{k}_f \left| V(-\tilde{G}_o^{(f)} + \tilde{G}_o^{(f)} V \tilde{G}_o^{(f)} - \ldots.) V_{\vec{r}_p} (1 - \tilde{G}_o^{(i)} V + \tilde{G}_o^{(i)} V \tilde{G}_o^{(i)} V - \ldots) \right| \vec{k}_i \right\rangle$$

$$t^{(2)} = -(2\pi)^2 m \left\langle \vec{k}_f \left| V(-\tilde{G}_o^{(f)} + \tilde{G}_o^{(f)} V \tilde{G}_o^{(f)} - \ldots) V (1 - \tilde{G}_o^{(i)} V + \tilde{G}_o^{(i)} V \tilde{G}_o^{(i)} V - \ldots) \right| \vec{k}_i \right\rangle ,$$

with $\tilde{G}_o^{(i)}$, $\tilde{G}_o^{(f)}$ corresponding to the initial and final energy, respectively. $t^{(1)}$ and $t^{(2)}$ are essentially the half-off-shell t-matrices which were considered in the 2-nd point. $t^{(1)}(\vec{r}_p)$ and $t^{(2)}(\vec{r}_p)$ are similar quantities, but because of the appearence of $V_{\vec{r}_p}$ they require evaluation of slightly modified impact parameter integrals than these which are needed for $t^{(1)}$ and $t^{(2)}$. For example, we have :

$$\frac{\partial}{\partial z_t} t^{(1)}(\vec{r}_p) = -2\eta_i k_i Z_t^{-1} \exp(-i r_{\parallel} \delta) \int_0^{\infty} db\, b\, J_o(b\Delta) K_o\left[(b^2 + s^2 - 2bs\cos\varrho)\delta\right] b^{2i\eta_i} \tag{5.13}$$

with $r_{\parallel} = \vec{r}_p \cdot \vec{k} k^{-1}$, $\delta = k_{f_\parallel} - k_{i_\parallel} = \varrho (1+\varrho^2)^{-1/2} \left| \vec{k}_f - \vec{k}_i \right|$, $\vec{s} \equiv (\vec{r}_p)_\perp$, φ- the angle between $r_{p\perp}$ and $(\vec{k}_f - \vec{k}_i)_\perp$ and $= \left| \vec{k}_f - \vec{k}_i \right|_\perp$.

It can be shown, that for large values of the Sommerfeld parameter the final result for the integral in Eq. (5.13) is similar to the corresponding one for $t^{(1)}$ and can be obtained from the latter one by the substitution :

$$\left| \vec{k}_f - \vec{k}_i \right|^2 \longrightarrow \left| \vec{k}_f - \vec{k}_i \right|^2 \left[1 - \varrho^2 (1+\varrho^2)^{-1} \eta_i^{-1} \vec{r}_p \cdot (\vec{k}_f - \vec{k}_i)_\perp \right] . \qquad (5.14)$$

However, for large $\eta \gg 1$, φ is very small, and with a good approximation may be neglected in Eq. (5.14). The main dependence on $\vec{r}_p$, then remains in Eq. (5.13) in the factor $\exp(-i r_{\parallel} \delta)$. This factor is expanded in the power series :

$$\exp(-i r_{\parallel} \delta) = \sum_L (-i r_{\parallel} \delta)^L (L!)^{-1} , \qquad (5.15)$$

and a specific transition with multipolarity L, is weighted by δ^L. The powers of $r_{\parallel} \delta$ can be better understood if we write :

$$r_{\parallel} \delta = r_{\parallel} (k_{f_\parallel} - k_{i_\parallel}) = (\tfrac{4}{3}\pi)^{1/2} r_p \varrho (1+\varrho^2)^{-1/2} \left| \vec{k}_f - \vec{k}_i \right| \sum_m Y^*_{lm}(\tfrac{\vec{k}}{k}) Y_{lm}(\tfrac{\vec{r}_p}{r_p}) . \qquad (5.16)$$

Then, returning to Eq. (5.9) we see that in the matrix element for Coulomb excitation there will be factors of the type :

$$\left\langle \varphi_f(\vec{r}_p) \left| r_p^L Y_{LM}(\frac{\vec{r}_p}{r_p}) \right| \varphi_i(\vec{r}_p) \right\rangle \sim \sqrt{B(EL)} , \qquad (5.17)$$

determined by the reduced transition probabilities of multipolarity L for the target nucleus. Numerical evaluations of the Coulomb excitation matrix elements for either α or ^{16}O scattered on ^{208}Pb are currently investigated by Goldfarb and one of the present authors[5.1]. This method may be also extended to two-step processes and applied to the evaluation or reorientation effects.

5.2. - Transfer reactions in the DWBA scheme with the eikonal distorted waves. -

Here, we are considering heavy-ion transfer reactions well above the Coulomb barrier. The conventional DWBA calculations are very laborious because of very many partial waves and a simplification of the 6-dimensional DWBA integral by neglecting the recoil is forbidden, because recoil plays and essential role at higher energies, as it was noted in Chapter 3.

To simplify the DWBA codes at energies well above the Coulomb barrier Da Silveira, Galin and Ngo[5.3] proposed to evaluate distorted waves in the eikonal approximation. In addition they neglected recoil and assumed a localization approximation. These additional assumptions, especialy the first one should not be made at higher energies, but Da Silveira et al. wanted to have simpler expressions to handle, and on such expression they tested their DWBA-high-energy scheme. The formula for the nucleon transfer differential cross section is the one proposed by Buttle and Goldfarb[5.4], and given explicitly in Chapter 3. Furthermore, Da Silveira et al. assumed that for high incident energy the Q-value of the reaction is small compared to energy, so they put $k_i \approx k_f \approx k$, and they disregarded differences between optical potentials in the initial and final channels, putting :

$$V^{i}_{opt}(r_i) \approx V^{f}_{opt}(r_f) = \overline{V}_{opt}(r). \tag{5.18}$$

Then, the product of the initial and final distorted waves is calculated in the eikonal scheme :

$$\chi^{(+)}(\vec{k}_i, \vec{r})\, \chi^{(-)*}(\vec{k}_f, \vec{r}) \approx \exp\left[i\vec{q}\cdot\vec{b} - i(\hbar v)^{-1} \int_{-\infty}^{\infty} \overline{V}_{opt}(r)\, dz' \right], \tag{5.19}$$

where $|\vec{q}| = 2k \sin\frac{\theta}{2}$ and $\vec{b}$ is connected with $\vec{r}$ by $\vec{r} = \vec{b} + \vec{k} k^{-1} z$.

The simplification achieved on the r.h.s. of Eq. (5.19) enables to write an expression on $T_{l\lambda}(\theta)$ defined in Chapter 3 in the form of a one-dimensional impact parameter integral:

$$T_{l\lambda}(\theta) \approx Y_{l\lambda}\left(\frac{\pi}{2}, 0\right) \int_0^{\infty} db\, b\, J_{\lambda}(qb) K_0\left(\sqrt{2mB_2\hbar^{-2}}\, b\right) n(b), \tag{5.20}$$

with :

$$n(b) = \exp\left[-i(\hbar v)^{-1} \int_{-\infty}^{\infty} \overline{V}_{opt}(r)\, dz \right], \qquad l+\lambda \text{ even},$$

and J_{λ}, K_0 are cylindrical and second order Bessel functions. Taking advantage of the localization approximation, one can use an asymptotic behaviour of K_0 and put in (5.20) :

$$K_0\left(\sqrt{2mB_2\hbar^{-2}}\, b\right) \simeq \left[\exp\left(-\sqrt{2mB_2\hbar^{-2}}\, b\right)\right] b^{-1/2}. \tag{5.21}$$

In Figs. 5.1 and 5.2 we show the results of Da Silveira et al.[5.3] for the transfer reactions induced by the ^{14}N projectiles on the Ag target. The distorting optical potential was found by fitting the elastic scattering data; various forms of the nuclear part of the potential were tried. As it seen, apart from the region of small angles, the agreement between theory and experiment is quite good.

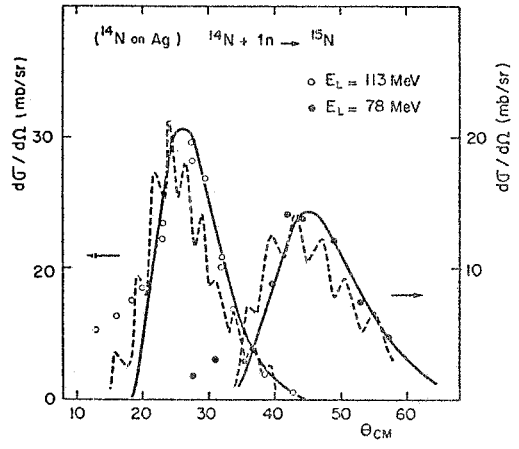

FIG. 5.1. - Neutron pick-up reaction at 78 and 113 MeV. Curves are the result of theoretical calculations using two well shapes; square (dashed curve) and Saxon-Woods (full curve) - Ref. (5.3). Experimental data are from Ref. (5.5).

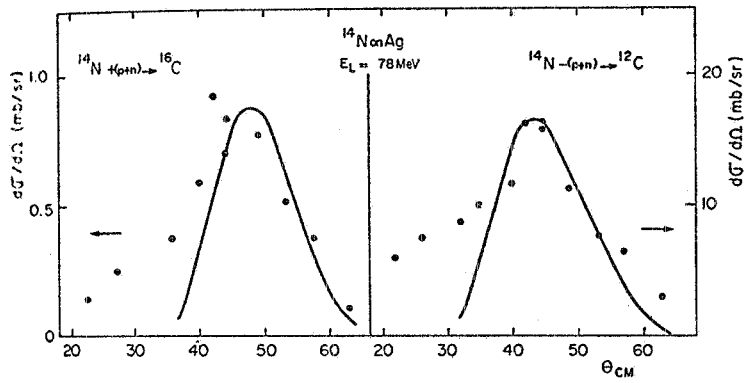

FIG. 5.2. - Two-nucleon (proton and neutron) transfer reaction: pick-up (left) and stripping (right). Curves are the result of theoretical calculations using a Saxon-Woods potential - Ref. (5.3). Experimental data are from Ref. (5.5).

5.3. - Heavy ion transfer reactions in an eikonal scheme, without DWBA. -

The formalism presented in this paragraph is an extension to the transfer reactions of the scheme described in 4.4. It is currently investigated numerically, so we shall give only the main formulae and state our motivations.

Our aims are:

a) Include a 3-body description in transfer processes $(c_1, t) + c_2 \rightarrow c_1 + (c_2, t)$ where the three "bodies" are c_1, c_2, and t (see Fig. 3.6 - pag. 23);

b) Include recoil and most of the 3-body kinematics, except for the internal motion in the target;

c) Avoid a partial wave expansion in the relative motion of ions by introducing the impact parameter representation;

d) Benefit from the simplicity of the eikonal formalism, but in such a form that it works for an arbitrary scattering angle and energy, i.e. use eikonal only for the evaluation of a correction to the exact, analytic solution.

These aims are realized by starting from the definition of the 3-body transition operators. It is useful, and a common practice among people doing 3-body calculations, to denote the three particles and the three possible 2-body bound states by the same index α, β, γ. So, the particle α, like c_2, is approaching the bound state $(\beta, \gamma) = \alpha$ like (c_1, t) and in the final state emerges particle β, like c_1, and the bound state $(\alpha, \gamma) = \beta$, like (c_2, t).

Then, if 2-body interactions between the three pairs are denoted as V_α, V_β, V_γ, corresponding to the pairs (β, γ), (α, γ) and (α, β), respectively, and:

$$\overline{V}_{\alpha,\beta} = V - V_{\alpha,\beta} \quad , \qquad V = \sum_{\alpha=1}^{3} V_\alpha \quad , \tag{5.22}$$

the 3-body transition operator describing the process:

$$\alpha + (\beta, \gamma) \longrightarrow \beta + (\alpha, \gamma) \quad ,$$

is:

$$T_{\beta\alpha} = \left\langle \phi_\beta \middle| \overline{V}_\beta \middle| \psi_\alpha^{(+)} \right\rangle = \left\langle \psi_\beta^{(-)} \middle| \overline{V}_\alpha \middle| \phi_\alpha \right\rangle \quad , \tag{5.23}$$

where $\phi_{\alpha,\beta}$ are the channel wave functions in the initial, final state made out of a plane wave associated with α, β, respectively and the bound state wave function (β,γ) and (α,γ) correspondingly, and $\psi_{\alpha,\beta}$ are the wave functions corresponding to the interaction in the initial, final state, respectively.

To evaluate $\psi_{\alpha,\beta}$ one either simplifies the procedure and treats the elastic scattering processes :

$$\alpha + (\beta,\gamma) \rightarrow \alpha + (\beta,\gamma) ,$$
$$\beta + (\alpha,\gamma) \rightarrow \beta + (\alpha,\gamma) , \qquad (5.24)$$

in a quasi-2-body spirit, and applies the scheme given in the subsection 4.4, or treats elastic processes (5.24) consistently in the 3-body framework, and evaluates the 3-body eikonal Green function first neglecting the relative motion in the (β,γ) or (α,γ) system, and then averaging over the wave function of these states. In the 2-nd approach we work with potentials V_β and V_γ for the first process, and V_α and V_γ for the second process, instead of an effective potential between α and (β,γ), and β and (α,γ), as it is in the 1-st case.

Having $\psi_{\alpha,\beta}$ in the impact parameter representation we evaluate integrals in Eq. (5.23) numerically. Of course the potentials $V_{\alpha,\beta,\gamma}$ must be determined first, either from the existing fits, or from new fits using the scheme given in the subsection 4.4 for pairs (β,γ); (α,γ) and (α,β) respectively. The matrix element in Eq. (5.23) contains either 3-dimensional, or 4-dimensional integrals, depending on the way we treat the eleastic processes (5.24). In any case we gain in comparison with the full DWBA scheme which preserves the recoil, incorporating many 3-body aspects of transfer processes, except for the internal motion in the bound systems in processes (5.24), which is only treated in an averaged way. A nice feature of this method is that it is not bounded to either small angles, or large energies. It should provide a scheme in which we can study the dynamics of heavy ion processes consistently at various energies.

5.4. - Faddeev-Lovelace equations in the eikonal approximation. -

Finally, we come to an eikonal scheme in which one does not write the solution for transition operators, but integral equations for these quantities. Such a scheme can incorporate 3-body dynamical effects in all possible configurations, without some averaging procedure which was needed before in discussing processes (5.24). However, this is done on the expense of solving integral equations. The eikonal technique serves two purposes. First, to simplify the Green function, second, to bypass partial wave expansion.

To make this program more definite we briefly mention the work of Janev and Salin[5.6] where a non-stationary scattering theory was used together with the straight-line eikonal approximation. The channel wave functions are taken as :

$$\tilde{\Phi}_\alpha = \varphi_\alpha(\vec{x}) \exp\left[-iE_\alpha t - ip\vec{v}\cdot\vec{r} - i(2m_3)^{-1} p^2 v^2 t\right] ,$$
$$\tilde{\Phi}_\beta = \varphi_\beta(\vec{s}) \exp\left[-iE_\beta t + iq\vec{v}\cdot\vec{r} - i(2m_3)^{-1} q^2 v^2 t\right] , \qquad (5.25)$$

with $\vec{x} = \vec{r}_{32}$, $\vec{s} = \vec{r}_{31}$, $\vec{r}_{ij} = \vec{r}_i - \vec{r}_j$, $p = \dfrac{m_1 m_3}{m_1+m_2}$, $q = \dfrac{m_2 m_3}{m_1+m_2}$, $\vec{v}$ - the relative velocity of the incoming particle and the target in the initial channel, $\varphi_\alpha(\vec{x})$, $\varphi_\beta(\vec{s})$ the eigenfunctions for the bound states of particles (1+3), and (2+3), respectively, and $E_{\alpha,\beta}$ the corresponding eigen-energies. In the straight-line eikonal approximation we have :

$$\vec{r} = \vec{r}(t) = \vec{b} + \vec{v}t ,$$

where t denotes time.

Janev and Salin defined appropriate 3-body transition operators and wrote the Faddeev--Lovelace integral equations for these operators. The structure of these equations is similar to the standard 3-body equations, however an important simplification, caused by the eikonal approximation is the reduction of dimensions of integration from 6 to 3+1. An by-product of the work of Janev and Salin is an explicit dependence on one potential of a transition operator evaluated in the approximation when only two of potentials are kept and one is set equal to zero. The whole influence of the 3-rd potential reduces merely to a phase factor:

$$\exp\left(-i \int_{-\infty}^{+\infty} V_3(t)\, dt\right) .$$

This is an important result in connection with our discussion in the previous subsection, where one of the interaction was only partially included in the wave function over which the processes (5.24) were averaged.

REFERENCES. -

(5.1) - L. J. B. Goldfarb and J. M. Namysłowski, Manchester preprint (to be published).
(5.2) - W. F. Ford, Jnl. Math. Phys. 7, 626 (1966).
(5.3) - R. Da Silveira, J. Galin and C. Ngo, Nuclear Phys. A159, 481 (1970).
(5.4) - P. J. A. Buttle and L. J. B. Goldfarb, Nuclear Phys. 78, 409 (1966).
(5.5) - J. Galin et al., Nuclear Phys. A159, 461 (1970).
(5.6) - R. K. Janev and A. Salin, Ann. Phys. 73, 136 (1972).

ACKNOWLEDGEMENT. -

One of the Authors (J. M. N.) would like to acknowledge Prof. G. Bellettini for a kind invitation and hospitality in the Frascati National Laboratories.